

Extremes and Short-Term Fluctuations in Coastal Ocean Acidification and Hypoxia



Key Points:

- A 20-year submesoscale-permitting simulation describes acidification and hypoxia hotspots along the U.S. West Coast in spatio-temporal detail
- Physical transport mitigates seasonal oxygen and pH decline in Central California but promotes it along the northern coast
- Short-term fluctuations in transport limit the duration of individual hypoxia and acidification events but exacerbate their intensity

Supporting Information:

Supporting Information may be found in the online version of this article.

Correspondence to:

P. Damien,
pdamien@ucla.edu

Citation:

Damien, P., Bianchi, D., Kessouri, F., & McWilliams, J. C. (2024). Extremes and short-term fluctuations in coastal ocean acidification and hypoxia. *Journal of Geophysical Research: Oceans*, 129, e2024JC021197. <https://doi.org/10.1029/2024JC021197>

Received 9 APR 2024

Accepted 4 NOV 2024

Author Contributions:

Conceptualization: Pierre Damien, Daniele Bianchi, Faycal Kessouri, James C. McWilliams

Formal analysis: Pierre Damien

Funding acquisition: Daniele Bianchi, James C. McWilliams

Investigation: Pierre Damien, Daniele Bianchi, James C. McWilliams

Methodology: Pierre Damien

Software: Pierre Damien, Faycal Kessouri

Validation: Pierre Damien, Faycal Kessouri





Writing – original draft: Pierre Damien

Writing – review & editing:

Pierre Damien, Daniele Bianchi, James C. McWilliams

© 2024. The Author(s).

This is an open access article under the terms of the [Creative Commons Attribution License](#), which permits use, distribution and reproduction in any medium, provided the original work is properly cited.

Pierre Damien¹ , Daniele Bianchi¹ , Faycal Kessouri^{1,2} , and James C. McWilliams¹ 

¹Department of Atmospheric and Oceanic Sciences, University of California, Los Angeles, CA, USA, ²Southern California Coastal Water Research Project, Costa Mesa, CA, USA

Abstract In Eastern boundary upwelling systems, such as the California Current System (CCS), seasonal upwelling brings low oxygen and low pH waters to the continental shelf, causing ocean acidification and hypoxia (OAH). The location, frequency, and intensity of OAH events is influenced by a combination of large-scale climatic trends, seasonal changes, small-scale circulation, and local human activities. Here, we use results from two 20-year long submesoscale-resolving simulations of the Northern and Southern U.S. West Coast (USWC) for the 1997–2017 period, to describe the characteristics and drivers of OAH events. These simulations reveal the emergence of hotspots in which seasonal declines in oxygen and pH are accompanied by localized short-term extremes in OAH. While OAH hotspots show substantial seasonal variability, significant intra-seasonal fluctuations occur, reflecting the interaction between low- and high-frequency forcings that shape OAH events. The mechanisms behind the seasonal decreases in pH and oxygen vary along the USWC. While remineralization remains the dominant force causing these declines throughout the coast, physical transport partially offsets these effects in Southern and Central California, but contributes to seasonal oxygen loss and acidification on the Northern Coast. Critically, the seasonal decline is not sufficient to predict the occurrence and duration of OAH extremes. Locally enhanced biogeochemical rates, including shallow benthic remineralization and rapid wind-driven transport, shape the spatial and temporal patterns of coastal OAH.

Plain Language Summary As the global ocean undergoes significant oxygen depletion and acidification due to increasing anthropogenic pressures, coastal areas are increasingly exposed to stressful conditions for marine ecosystems. Eastern boundary upwelling systems, as the California Current System, are naturally vulnerable due to the seasonal on-shelf transport of nutrient-rich, oxygen-poor, and acidic waters. In this study, we analyze a 20-year high-resolution numerical simulation of the southern and northern U.S. West Coast to describe the characteristics and drivers of ocean acidification and hypoxia events. These simulations reveal the emergence of hotspots characterized by significant increases in the frequency and duration of acidification or hypoxia events. While these locations show substantial seasonal variability, there is also significant intra-seasonal variability, reflecting the interaction of low- and high-frequency forcings that shape extreme events. Critically, the seasonal decrease is not sufficient to predict the occurrence and duration of extreme events. The influence of short-term fluctuations in transport and remineralization rates is twofold, as they significantly increase the frequency and severity of extreme events, but also lead to shorter individual events. The resulting impacts on marine organisms are difficult to predict, as high-frequency variability exacerbates potentially harmful conditions, but also causes periods of relaxation that may promote ecosystem resilience.

1. Introduction

The global ocean is undergoing significant oxygen loss and acidification due to increasing anthropogenic pressure (Doney et al., 2009; Levin, 2018). Over the past 60 years, the global loss of oceanic oxygen (O_2) has exceeded 2% per decade (Schmidtko et al., 2017) and the global surface pH has dropped by approximately 0.005 pH units per decade (Feely et al., 2009). This trend is expected to continue (IPCC, 2023) and intensify under increasing ocean warming and stratification (Li et al., 2020). Together with increasing temperatures, O_2 loss and acidification are major stressors to ocean ecosystems, which depend on specific O_2 and pH ranges for their functioning and composition (Deutsch et al., 2015; Orr et al., 2005). Low O_2 conditions alter a wide range of physiological, metabolic, and behavioral aspects of marine life, especially for demersal and benthic organisms that live near or within the seabed (Service, 2004), and affect elemental cycles that depend on aerobic respiration (Breitburg et al., 2018; Levin, 2018). In parallel, calcification rates and other biological functions can be impaired by

declining pH, for both calcifying and non-calcifying organisms (Fabry et al., 2008; Hauri et al., 2009). While low-O₂ and acidification thresholds vary by organism, and are likely modulated by temperature, extreme reductions in oxygen and pH can be lethal to marine organisms, with potentially synergistic effects (Gruber et al., 2021). Repeated exposure to OAH thus poses a risk to marine ecosystems, especially those with slower adaptive capacity than the timescale of environmental change (Bednaršek et al., 2017).

Coastal waters are particularly vulnerable to the emerging risks of OAH. Because of enhanced exchanges with adjacent lands, the overlying atmosphere, and the sediment, biogeochemical rates are intensified (Damien, Bianchi, McWilliams, et al., 2023; Muller-Karger et al., 2005) and the effects of climate change amplified (Fennel & Testa, 2019; Laruelle et al., 2018) on continental shelves. Coastal waters are naturally exposed to O₂ loss and pH reductions, in particular in eastern boundary upwelling systems characterized by seasonal on-shelf transport of nutrient-rich, O₂-poor, and acidic waters (Feely et al., 2008). Intense primary production and remineralization amplify subsurface oxygen loss and acidification, in particular on continental shelves exposed to nutrient inputs and eutrophication from natural (Rabalais et al., 2002; Zhou et al., 2017) and anthropogenic sources (Kessouri, McWilliams, et al., 2021; Laurent et al., 2017). The combination of naturally occurring low-O₂ and low-pH waters and intense variability in ocean circulation (Dauhajre et al., 2017), water residence time (Fennel & Testa, 2019; Liu et al., 2019), biogeochemical rates (Damien, Bianchi, McWilliams, et al., 2023), air-sea fluxes (Resplandy et al., 2024), and anthropogenic nutrient inputs (Cai et al., 2011; Kessouri, McWilliams, et al., 2021; Liu et al., 2021) makes continental shelves particularly prone to extreme OAH conditions (Fennel & Testa, 2019).

The CCS has a rich history of OAH studies based on both observations and numerical models. Several instances of hypoxic and low-pH conditions have been documented in the region, in particular along the coasts of Vancouver Island (Franco et al., 2023), Washington State (Barth et al., 2024; Connolly et al., 2010), Oregon (Adams et al., 2013, 2016; Chan et al., 2008; Hales et al., 2006; Harris et al., 2013), and California (Booth et al., 2012; Feely et al., 2008; McClatchie et al., 2010). Detrimental impacts of OAH on marine organisms have already been observed in the CCS (Bednaršek et al., 2014, 2017; Feely et al., 2016; Haigh et al., 2015; McClatchie et al., 2010), including habitat compression for zooplankton and fish (Bednaršek & Ohman, 2015; Howard et al., 2020).

While multiple modeling studies have focused on future OAH projections and long term trends (Gruber et al., 2012; Hauri, Gruber, Vogt, et al., 2013), the importance of basin-scale interannual to decadal climate variability in modulating OAH is also well recognized (Desmet et al., 2023; Deutsch et al., 2011; Turi et al., 2016). Recent work has shown significant regional effects of large-scale climate modes superimposed on anthropogenic trends, highlighting regions along the coast that are particularly exposed to severe OAH (Chan et al., 2017; Cheresh & Fiechter, 2020; Feely et al., 2024).

The prevalence of upwelling imparts a seasonal timescale to OAH along the USWC. However, observations show that intense OAH events can occur on shorter timescales, ranging from several hours to days and weeks (Adams et al., 2013, 2016; Connolly et al., 2010; Hales et al., 2006; Harris et al., 2013). Although seasonal, interannual, and decadal variability modulate such events, their occurrence remains short-term and episodic. A useful framework to analyze OAH thus focuses on “extremes” or “events” (Burger et al., 2020; Gruber et al., 2021) which describe OAH patterns based on their duration, frequency, intensity, and spatial extent. This framework is particularly relevant to OAH impacts on marine organisms (Frieder et al., 2014) and accommodates the occurrence of compound events (Bednaršek et al., 2016; Feely et al., 2018; Gruber et al., 2021; Walter et al., 2024), when hypoxia and acidification overlap, amplifying the risk of ecosystem harm.

Because of limitations in spatial coverage and sampling frequency, a coast-wide characterization of OAH events cannot be based on observations alone but must also rely on numerical models. Regional modeling studies have yielded fundamental insights on the patterns and variability of OAH in the CSS (Bednaršek et al., 2021; Cheresh et al., 2023; Desmet et al., 2022, 2023; Hauri, Gruber, McDonnell, & Vogt, 2013; Kroeker et al., 2023). However, compound events remain poorly characterized. Accurate modeling of OAH extremes on scales relevant to coastal ecosystems requires submesoscale-resolving models driven by high-frequency atmospheric forcings, with a realistic representation of nutrient, carbon, and oxygen cycles (Damien, Bianchi, McWilliams, et al., 2023; Damien, Bianchi, Kessouri, & McWilliam, 2023).

In this study, we investigate OAH extremes along the USWC shelf, with a specific focus on event duration. Our work is based on two 20-year-long numerical simulations of the Northern and Southern CCS with a submesoscale-resolving physical-biogeochemical model driven by realistic atmospheric forcings. The extended

duration of our simulations enables robust statistical analysis of OAH events. We also leverage the extensive data sets of biogeochemical observations collected in this region by numerous programs, which enables a thorough validation of the model. We first examine the distribution, duration, and frequency of individual and compound OAH events. We then identify the processes that drive shelf habitats below specific OAH thresholds and characterize the seasonal and intra-seasonal timescales of these drivers.

The rest of the paper is organized as follows. Section 2 details the configuration of the numerical simulations, defines the metrics of OAH exposure, and describes the framework used to diagnose OAH extremes and short-term fluctuations. Section 3 validates the model against in situ measurements, characterizes the variability of OAH extremes, and investigates the processes controlling the onset and termination of OAH events at seasonal and sub-seasonal timescales. Section 4 discusses the main findings and concludes the paper.

2. Methods

2.1. Physical-Biogeochemical Model

We use the UCLA version of the Regional Ocean Modeling System (ROMS) (Shchepetkin & McWilliams, 2005) coupled online to the Biogeochemical Elemental Cycling model (BEC) (Deutsch et al., 2021; Moore et al., 2004). ROMS solves the hydrostatic primitive equations that describe the conservation of momentum, temperature and salinity, and the transport of biogeochemical tracers in a terrain-following coordinate system. BEC represents the biogeochemical cycles of six major elements (C, P, N, Si, Fe, and O) resulting from the interaction of three phytoplankton and one zooplankton groups.

The oxygen cycle includes production by photosynthesis and consumption by respiration of dissolved and particulate organic matter and nitrification. The carbon cycle includes a representation of the carbonate system based on dissolved inorganic carbon (DIC) and alkalinity. DIC and alkalinity are altered by photosynthesis, remineralization, and formation and dissolution of particulate calcium carbonate (CaCO_3). At the surface, air-sea fluxes of oxygen and carbon dioxide are computed based on the gas-exchange parameterization by Wanninkhof (1992). Oxygen respiration in the sediment is linked to the remineralization of organic carbon that settles and accumulates at the bottom, following the carbon-to-oxygen Redfield ratio. A detailed description of BEC model's equations and parameters can be found in Deutsch et al. (2021).

The model was run on two overlapping Arakawa C grids for the Northern and Southern CCS (USWC-N and USWC-S, respectively, see Figure 1), with a horizontal resolution of 1 km and 60 stretched vertical levels (Damien, Bianchi, McWilliams, et al., 2023; Kessouri, Bianchi, et al., 2020). We consider this configuration submesoscale-permitting because it allows the emergence of submesoscale dynamics (Capet et al., 2008; Damien, Bianchi, Kessouri, & McWilliams, 2023; Kessouri, Bianchi, et al., 2020). Initial and boundary conditions are obtained by dynamical downscaling of a similar parent simulation run at 4 km (Deutsch et al., 2021; Renault et al., 2021). Surface forcing are computed at 6 km resolution from bulk formulae applied to hourly output from an atmospheric simulation with the Weather Research and Forecasting Model (WRF) model (Skamarock et al., 2008). Further details on the 4-km parent configuration setup, initialization, and boundary forcings can be found in Deutsch et al. (2021) and Renault et al. (2021), along with an extensive validation of the large-scale circulation and biogeochemical solutions. Analyses of nutrient, carbon, and oxygen cycles on the USWC continental shelf based on the Northern and Southern 1-km simulations are presented in Kessouri et al. (2020a), Damien, Bianchi, McWilliams, et al. (2023) and Damien, Bianchi, Kessouri, and McWilliams (2023).

The two 1-km configurations are run for over 20 years, covering the 1997–2017 period, and analyzed jointly. Output is saved as daily averages for model velocities and tracers, and as monthly averages for physical transport fluxes and biogeochemical reaction rates. This output frequency allows us to diagnose the distribution of OAH events and the seasonal balance of biogeochemical tracers. We further investigate the role of high-frequency processes for OAH extremes by using daily averages of physical transport and biogeochemical rates for the year 2001.

We focus our analysis on the continental shelf, here defined as ocean bottom depths shallower than 200 m (Laruelle et al., 2013). To facilitate analysis of alongshore patterns, we remapped model variables and fluxes on a curvilinear, along-isobath coordinate system that uses isobaths between 0 and 200 m depth as the \vec{x} axis and

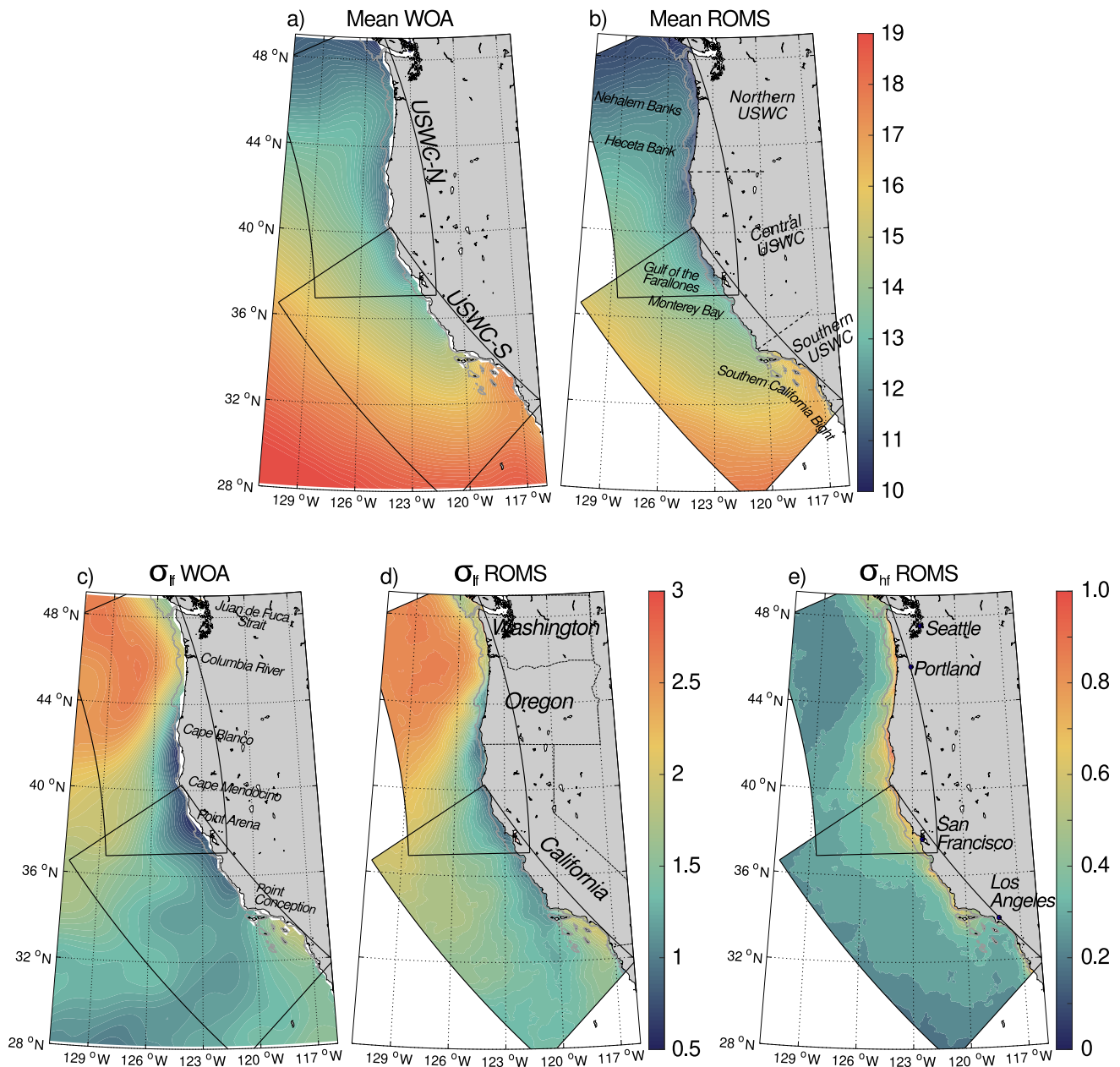


Figure 1. Mean sea surface temperature (SST in °C) for (a) the World Ocean Atlas (WOA) (Locarnini et al., 2018) and (b) the numerical model (averaged over the 1997–2017 period). Seasonal variability of sea surface temperature (SST) computed as the root-mean square of the low-frequency fluctuations (σ_{lf} , Equation 2) in (c) the WOA and (d) the model. (e) Intra-seasonal variability in SST (σ_{hf} , Equation 2) in ROMS. The black boxes show the Northern and Southern USWC model domains, and the gray line the 200-m isobath, which separates coastal from offshore waters.

latitude as the \vec{y} axis (Damien, Bianchi, McWilliams, et al., 2023). This choice of coordinates naturally highlights alongshore variability and cross-shore gradients, particularly in regions characterized by a narrow and uneven shelf width.

2.2. OAH Exposure

We define OAH extreme events using a criterion based on absolute thresholds rooted on physiological and chemical considerations. Rather than using pH, we use the saturation state of the CaCO_3 mineral aragonite (Ω_{Ar}) as a metric of ocean acidification, consistent with prior work in the USWC (Chan et al., 2017; Desmet et al., 2022;

Harris et al., 2013; Turi et al., 2016). We define corrosive conditions as $\Omega_{Ar} < 1$. This is a widely accepted threshold that separate supersaturated from undersaturated waters relative to the aragonite form of CaCO_3 used by several calcifying organisms (Deutsch et al., 2021; Juranek et al., 2009). Below this threshold, calcifying organisms are exposed to acidic waters that can lead to shell dissolution and other detrimental effects (Bednaršek et al., 2017). As a quantity linked to the concentration of carbonate ions (CO_3^{2-}) in seawater, Ω_{Ar} is directly affected by changes in the excess of alkalinity relative to DIC (Sarmiento & Gruber, 2006).

We define hypoxic conditions as oxygen concentrations lower than 64.0 mmol m^{-3} ($\sim 2 \text{ mg L}^{-1}$). This is more restrictive than the value used by Deutsch et al. (2021) in the CCS, but similar to that used by Fennel et al. (2013) in the Northern Gulf of Mexico and Connolly et al. (2010) on the Oregon and Washington shelf. Oxygen loss below these concentration often excludes several marine aerobic organisms. We note that more accurate, albeit more complex, species-dependent hypoxic thresholds could be defined, for example, based on the Metabolic Index (Deutsch et al., 2015; Howard et al., 2020).

Following previous approaches (Burger et al., 2020; Gruber et al., 2021), we investigate periods during which, at any given location, O_2 or Ω_{Ar} drop under the selected thresholds. These periods are either referred to as hypoxic or acidification events, or, in short, extreme events. (We use these terms interchangeably throughout the paper.) We further quantify the frequency, duration, recurrence, and intensity of these events. Based on these metrics, we identify regions along the coast that are particularly sensitive to OAH extremes, which we refer to as OAH “hotspots.” A hotspot is defined as coastal area characterized by a marked increase in the frequency and duration of acidification or hypoxic events. Specifically, a region qualifies as a hotspot if it meets two criteria: (a) it experiences localized acidification or hypoxic extremes occurrence larger than the alongshore mean value and (b) the duration of the local prolonged extreme events (75th percentile) exceeds the alongshore mean.

The analysis is conducted in two steps: first, we investigate hypoxic and acidification events, and coastal hotspots, separately (Section 3.2); second, we investigate extreme events and hotspots characterized by simultaneous hypoxia and acidification, which we refer to as OAH extreme or compound events (Section 3.3). This metric-based approach provides objective benchmarks to quantify ecosystem exposure to extreme conditions. However, we recognize that specific impacts on marine organisms are often taxon-dependent (Bednaršek et al., 2019) and require additional biological translations (Frieder et al., 2023; Howard et al., 2020).

2.3. Ω_{Ar} Computation

Because Ω_{Ar} is not a state variable in BEC, we compute it offline with the CO2SYS carbon system algorithm (Van Heuven et al., 2011), using daily averages of DIC, alkalinity, silicate, phosphate, temperature, and salinity. For validation purpose and to address the limited numbers of direct carbon system observations along the USWC compared to other hydrographic variables (Jiang et al., 2021), we also use two empirical models of Ω_{Ar} , based on temperature and oxygen, specifically developed for the Oregon shelf (Juranek et al., 2009) and Southern CCS (Alin et al., 2012). The use of these empirical relationships has limitations regarding the period to which they are applied. Although they are considered robust over a period ranging from 10 years (Juranek et al., 2009) to 20 years (Alin et al., 2012), moving away from the calibration date (i.e., 2007) results in increasingly biased Ω_{Ar} estimates due to the progressive addition of anthropogenic carbon. When applied to the period of our study (1997–2017), Ω_{Ar} may exhibit significant biases toward the boundaries of this period. However, these empirical relationships are used solely for validation and comparison purposes in our study. Consequently, any biases related to a suboptimal algorithm use are consistent in both the model and in situ estimates, ensuring fair comparisons. Furthermore, the analysis of Ω_{Ar} temporal fluctuations and acidification events is based on computations that use the full carbonate system based on modeled tracer concentrations.

A comparison of modeled Ω_{Ar} with both direct observations and the empirical relationships reveals that the model is able to capture the spatial gradients and temporal variability in this quantity. However, the model systematically overestimates Ω_{Ar} by ~ 0.27 units (Text S1 in Supporting Information S1). Further comparisons with the GLODAPv2 database (Olsen et al., 2016) show that, although DIC and alkalinity are in good agreement with observations, modest biases ($< 2\%$) lead to the overestimate of Ω_{Ar} in the model.

We attribute these biases to the open boundary conditions for DIC and alkalinity imposed on the parent ROMS-BEC solution and discussed in Deutsch et al. (2021). In Deutsch et al. (2021), DIC and alkalinity from GLODAPv1 (Key et al., 2004), with a reference year of 1995, were used to generate boundary conditions by imposing

density- and time-dependent corrections to account for the oceanic invasion of anthropogenic DIC (Sabine et al., 2004). The slight overestimate of DIC and alkalinity in the model likely reflects limitations of this approach. Without correcting for the model overestimate of Ω_{Ar} , application of an absolute ocean acidification threshold to model output would result in an underestimate of the occurrence of acidification events. In order to correct the model bias, while preserving dynamically consistent spatial gradient and temporal variability, we apply an additive correction to the modeled DIC and alkalinity to align them with observations from GLODAPv2. This correction, which includes a weak zonal dependence, never exceeds 1.9% of the modeled DIC and alkalinity concentrations (see Figure S2 in Supporting Information S1). This adjustment significantly reduces the bias in Ω_{Ar} (Figure S1 in Supporting Information S1) and ensures an accurate representation of the temporal and spatial variability when compared against in situ data (see Section 3.1).

2.4. Diagnostics of OAH Variability and Its Driving Processes

We use the following metrics to characterize the mean state and variability of O_2 and Ω_{Ar} . For an arbitrary model variable x (here either O_2 or Ω_{Ar}), we define the long-term mean (\bar{x}) and the seasonal mean (\tilde{x}_i) respectively as:

$$\bar{x} = \frac{1}{n} \sum_{i=1}^n x_i \quad ; \quad \tilde{x}_i = \frac{1}{m} \sum_{j=i-\frac{m}{2}}^{i+\frac{m}{2}} x_j \quad ; \quad (1)$$

where $n = 20 \text{ years} \cdot 365 \text{ days}$, $m = 60 \text{ days}$, i and j are summation indices in days. We quantify the variability at specific time scales by using the following decomposition on the temporal variance of these quantities:

$$\sigma_{tot} = \sqrt{\frac{1}{n} \sum_{i=1}^n (x_i - \bar{x})^2} \quad ; \quad \sigma_{lf} = \sqrt{\frac{1}{n} \sum_{i=1}^n (\tilde{x}_i - \bar{x})^2} \quad ; \quad \sigma_{hf} = \sqrt{\frac{1}{n} \sum_{i=1}^n (x_i - \tilde{x}_i)^2}. \quad (2)$$

Here, σ_{tot} measures the total variability of daily averaged quantities, σ_{lf} the low-frequency variability associated with the seasonal cycle, and σ_{hf} the variability in the sub-seasonal range. We do not quantify long term trends and interannual variability, which are described elsewhere (Deutsch et al., 2021).

We diagnose the effect of seasonal and sub-seasonal processes on OAH, by considering the balance equations for O_2 and Ω_{Ar} . These can be summarized as follows:

$$\frac{\partial O_2}{\partial t} = PHY(O_2) + BGC(O_2) \quad ; \quad \frac{\partial \Omega_{Ar}}{\partial t} = PHY(\Omega_{Ar}) + BGC(\Omega_{Ar}). \quad (3)$$

In these equations, PHY represents the divergence of the physical transports by advection and diffusion and BGC represents biogeochemical sources and sinks. Unlike O_2 , Ω_{Ar} is not a prognostic model variable. Therefore, we estimate the balance terms for Ω_{Ar} with an offline calculation. A small fluctuation in $\Omega_{Ar}(DIC, Alk, T, \dots)$ can be approximated by a Taylor series expansion (Hauri, Gruber, Vogt, et al., 2013):

$$\Delta \Omega_{Ar} = \Omega_{Ar}(DIC + \Delta DIC, Alk + \Delta Alk, T + \Delta T, \dots) - \Omega_{Ar}(DIC, Alk, T, \dots) \quad (4)$$

$$= \frac{\partial \Omega_{Ar}}{\partial DIC} \Delta DIC + \frac{\partial \Omega_{Ar}}{\partial Alk} \Delta Alk + \frac{\partial \Omega_{Ar}}{\partial T} \Delta T + \dots + O(DIC^2, \Omega_{Ar}^2, T^2, \dots), \quad (5)$$

where T is temperature. Assuming small contributions from temperature and salinity, a quasi-linear relationship between Ω_{Ar} and the difference between alkalinity and DIC (a close approximation to the CO_3^{2-} ion concentration), $Alk - DIC$, can be derived (see Figure S3 in Supporting Information S1):

$$\Omega_{Ar} \approx \alpha(Alk - DIC) \quad \text{with} \quad \frac{\partial \Omega_{Ar}}{\partial Alk} \approx - \frac{\partial \Omega_{Ar}}{\partial DIC} = \alpha. \quad (6)$$

The equation shows that Ω_{Ar} can be interpreted as a measure of the deficit of DIC relative to alkalinity (Sarmiento & Gruber, 2006). Based on analysis of the model solution, we set $\alpha = 10^{-2} \text{ m}^3 \text{ mmol}^{-1}$ (see Figure S3 in

Supporting Information S1). While this linear approximation cannot be used to precisely evaluate the Ω_{Ar} budget closure, we find it accurate enough to evaluate the processes controlling its temporal variations, as further demonstrated in Supporting Information S1 (Figure S4). Based on Equation 6, we calculate $PHY(\Omega_{Ar})$ from α and $PHY(Alk) - PHY(DIC)$ and $BGC(\Omega_{Ar})$ from α and $BGC(Alk) - BGC(DIC)$.

In order to attribute the influence of fluctuations at frequencies higher than seasonal, we compare the statistics of OAH extreme events in two cases. In the first case, O_2 and Ω_{Ar} time-series are computed from daily physical fluxes and biogeochemical rates. In the second case, we reconstruct the time-series from the low-frequency tendency terms in Equation 3, so that their temporal evolution only reflects seasonal processes. Accordingly, for a model variable x (either O_2 or Ω_{Ar}), we set:

$$x_{tot}(t) = \int_0^t (PHY(x) + BGC(x)) dt + x(t_0), \quad (7)$$

$$x_{lf}(t) = \int_0^t (\widetilde{PHY}(x) + \widetilde{BGC}(x)) dt + x(t_0), \quad (8)$$

where x_{tot} and x_{lf} are the reconstructed timeseries with and without the inclusion of intra-seasonal variability respectively. The short-term fluctuations of physical fluxes are calculated by applying the high-pass seasonal filter as:

$$PHY' = PHY - \widetilde{PHY}. \quad (9)$$

3. Results

3.1. Model Evaluation

The model provides a realistic simulation of the mean sea surface temperature (SST) relative to the observed climatology from the World Ocean Atlas (Locarnini et al., 2018), with colder waters found nearshore along the Central and Northern California coasts (Figure 1). This SST pattern reflects coastal upwelling and is associated with low seasonal variance (σ_{lf}). While the model shows a slight positive bias in σ_{lf} along the coast, it accurately represents the larger values observed in the South California Bight and in the northwestern part of the domain. The SST variance in the sub-seasonal range (σ_{hf}) is significantly higher on the narrow continental shelf.

We assess modeled O_2 and Ω_{Ar} against an observational compilation of in situ observations from a variety of monitoring and scientific programs (see Text S2 in Supporting Information S1). Comparisons are first performed by considering temporal averages, to evaluate the spatial distribution of OAH properties, and then at 11 coastal stations characterized by extensive measurements, where we examine the seasonal cycles and the range of variability in O_2 and Ω_{Ar} . O_2 observations nearly cover the entire USWC coast at $1/3^\circ$ resolution and allow to construct surface and subsurface time-series at several coastal locations. In contrast, direct measurements of Ω_{Ar} are considerably less abundant. For regions with co-located DIC, alkalinity, silicate, phosphate, temperature, and salinity observations, we compute Ω_{Ar} based on the CO2SYS algorithm. For these calculations, we use corrected modeled DIC and alkalinity concentrations, as described in Section 2.3. For additional Ω_{Ar} validation in the context of limited numbers of direct observations of carbon system parameters, we compare modeled Ω_{Ar} time-series with Ω_{Ar} estimated from the empirical algorithms by Juraneck et al. (2009) and Alin et al. (2012). Results from the model validation are summarized in Figures 2 and 3. Additional time-series comparisons are shown in Supporting Information S1 (Text S2, Figures S6–S16), and several metrics are computed to statistically evaluate the model performance against observations (Text S2, Tables T1 and T2 in Supporting Information S1), following the methodology for model validation in Kessouri, McLaughlin, et al. (2021).

The model accurately represents the spatial distribution of O_2 and Ω_{Ar} along the USWC (Figures 2 and 3), in particular the low values along the coast and in the Southern California Bight, albeit with a weak negative bias. The relative average bias with respect to observations is -0.07 for O_2 and -0.13 for Ω_{Ar} . The discrepancy can be partially attributed to the use of 20-year means for the model, as compared to means of all the available observations, which are more sparse in time and more commonly collected during the upwelling season. The model

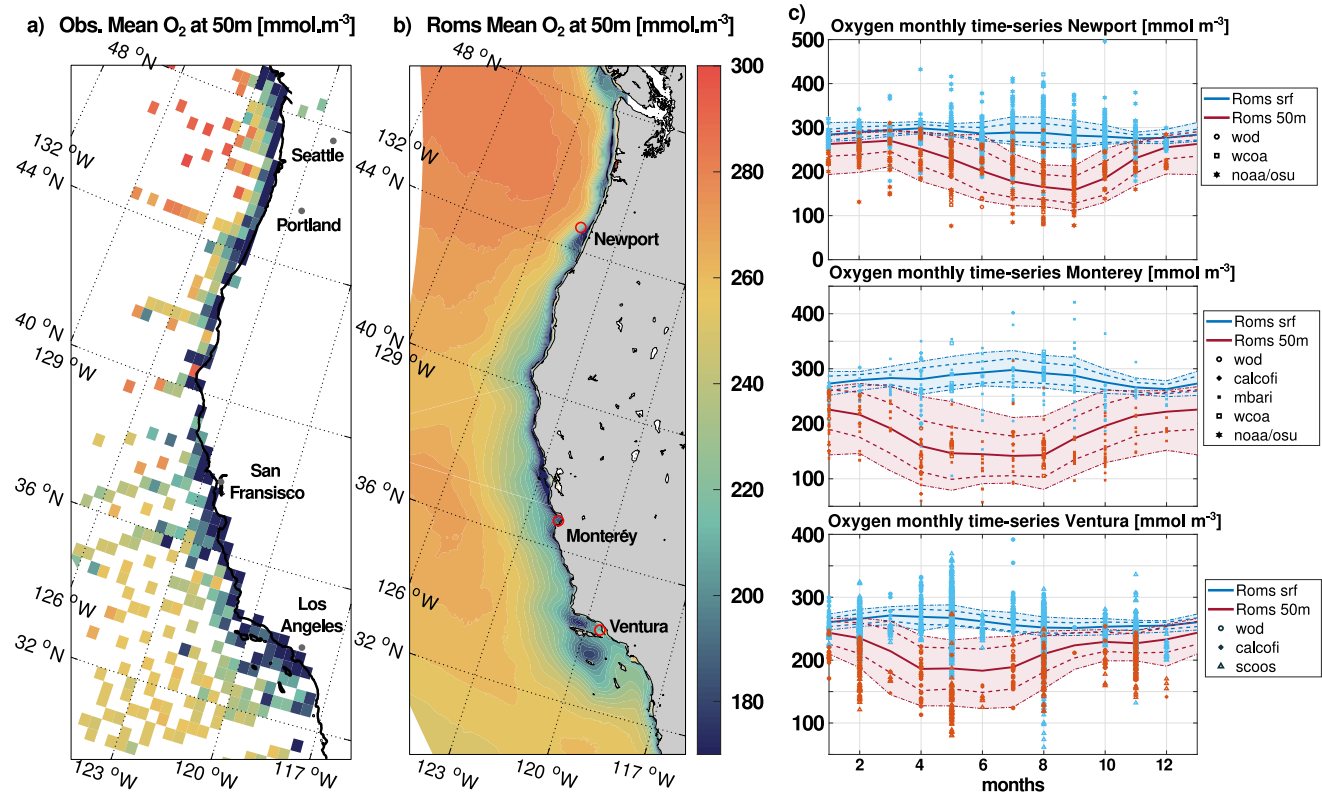


Figure 2. Comparison of modeled and observed O₂. Maps of mean O₂ at 50 m from (a) in situ observations and (b) the model averaged between December 1999 and November 2017. Observations were collected from various sources and gridded at 1/3° resolution. The 50 m isobath is shown by the dashed line. For waters shallower than 50 m, the mean O₂ field at the bottom is shown. (c) Seasonal cycle of O₂ at three locations along the USWC (shown as red circles): Newport (upper panel), Monterey Bay (middle panel), and Ventura (lower panel). The mean seasonal cycle (solid line) is shown along with the 1 standard deviation (dashed lines) and the 5th and 95th percentiles (color shading and dot-dashed lines) envelopes at the surface (blue) and at depth (red). Dots show concentrations observed across a 0.2° box centered at each location.

also captures the seasonal and intra-seasonal variability in O₂ and Ω_{Ar} in both surface and subsurface waters, with most measurements falling within the seasonal envelope of variability of the model (5%–95% percentiles).

Yet, observations also show a significant number of outliers relative to model predictions, suggesting somewhat weaker variability in the model. On average across the 11 stations evaluated, the ratio of the standard deviation of O₂ measurements to that of the corresponding model time series, RSD, is 2.00 at the surface and 0.82 at a depth of 50 m. At the surface, a reduced variability at high-frequencies could arise from model limitations, including use of daily averages, unresolved dynamics, and poorly represented physical processes such as tides and waves (Dauhajre et al., 2017; Hypolite et al., 2021). The lack of terrestrial nutrient inputs, both natural and anthropogenic, via river discharge and wastewater outfalls (Kessouri, McWilliams, et al., 2021) also limits the model's ability to capture coastal eutrophication and the associated biogeochemical effects, in particular in the Southern California Bight, Monterey Bay, and Gulf of Farallones. In a dedicated study based on a downscaled configuration of this solution, Kessouri, McLaughlin, et al. (2021) show that the inclusion of ocean outfalls improves the representation of modeled carbonate system and oxygen predictions. Furthermore, the relatively simple ecosystem representation in the model may not capture the full extent of phytoplankton blooms and their consequences (Van Oostende et al., 2018).

3.2. Emergence and Characteristics of Hotspots

We first focus on the continental margin and consider hypoxic and acidification events separately. Low O₂ and low Ω_{Ar} conditions are observed at several locations on the USWC continental shelf and around the Channel Islands in the Southern California Bight (Figures 2 and 3). These regions are characterized by significant temporal

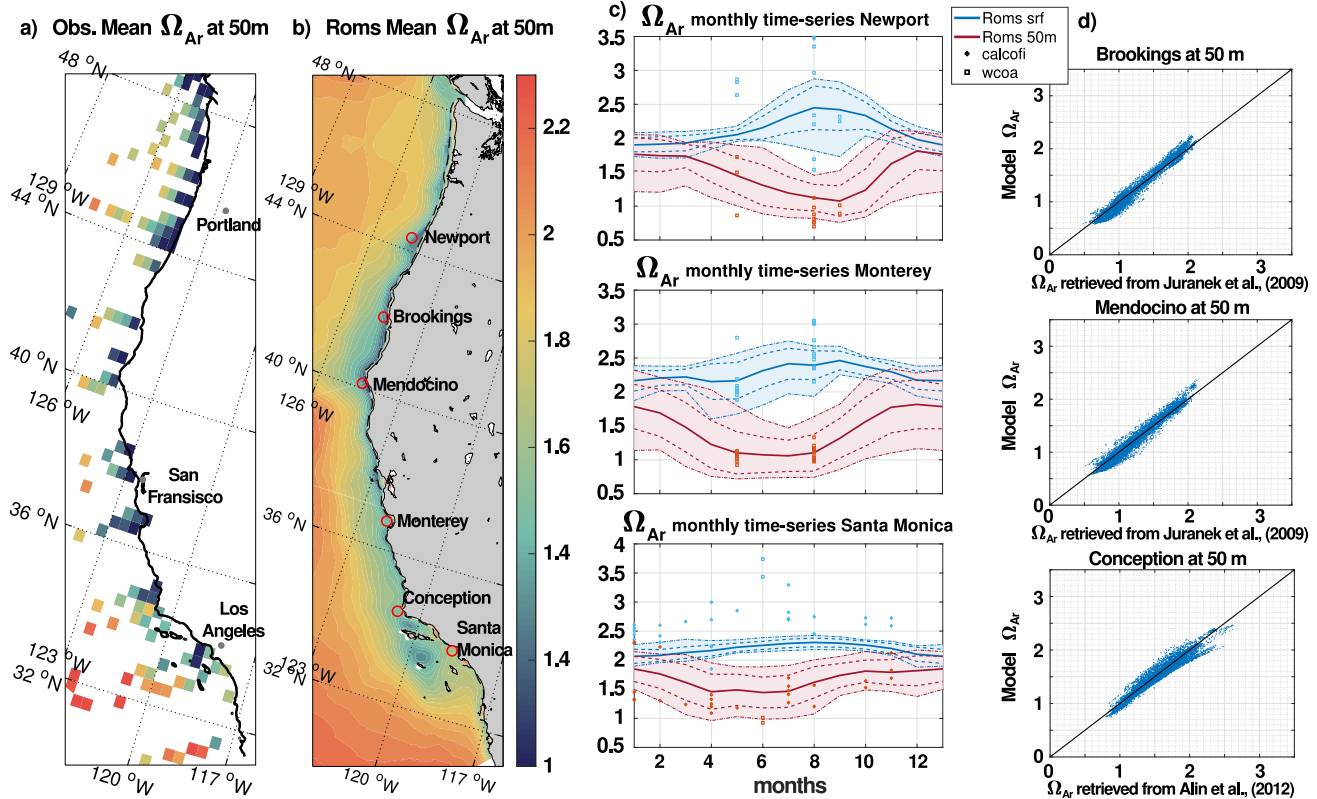


Figure 3. (a, b, and c) Same as Figure 1, but for Ω_{Ar} . The scatterplots in panel (d) compare Ω_{Ar} from the model with Ω_{Ar} calculated from observed temperature and O_2 by applying the empirical algorithms of Alin et al. (2012) and Juranek et al. (2009). Analyses are performed at three locations, indicated by red dots in panel (b).

variability associated with the seasonal cycle of upwelling (Figure 1c), which makes them particularly sensitive to the emergence of OAH.

The frequency of extreme events averaged across latitudinal bands (Figures 4a and 5a) reveals a greater incidence of acidification compared to hypoxia. The frequency of acidification events ranges from about 10^{-4} to 1, with the latter case corresponding to Ω_{Ar} persistently below a threshold of 1.0 for the entire 20-year simulation period. In contrast, the frequency of hypoxic event does not exceed 10^{-1} , that is, about 36 days each year. The thickness of permanently acidic layer expands from South to North, suggesting increasing vertical habitat compression for calcifying organisms along a meridional gradient. A similar, but less pronounced pattern is observed for O_2 , with more frequent subsurface hypoxia in the northern region. In the Southern California Bight, the occurrence of extreme events is limited, with hypoxia largely confined to waters deeper than 100 m. Shallower hypoxia sporadically develops in nearshore bottom waters characterized by intense benthic respiration. While subsurface extreme events are more common in the northern region, near-surface hypoxia and acidification are more frequently encountered in Central and Northern California, where upwelling is more intense.

Extreme OAH events shows notable regional patterns (Figures 4b and 5b). In the surface layer (0–50 m), the most recurring hypoxia is observed on the inner-shelf. Hypoxia on the outer shelf is only evident in Central California (north of Morro Bay and south of Cape Mendocino). Four alongshore sites stand out as major locations of hypoxia, with event frequency up to 0.1 (Figure 4b): the San Francisco coast extending from Monterey Bay to Bodega Bay, the Heceta Bank on the Oregon shelf, most of the Washington coast from the mouth of the Columbia River to Teahwhit Head, and the western shelf of Vancouver Island.

In contrast to hypoxia, acidification affects the shelf more evenly along a cross-shore gradient. Between California and Oregon (from Point Arena to Cape Blanco) the frequency of acidification events exceeds 0.2 (about 75 days per year) at 50 m depth over the entire shelf. Acidification is generally more uniform and persistent in the alongshore direction than hypoxia (Figure 5b). Sustained acidification, with frequencies exceeding 0.25, occurs over an extensive stretches of the coast, encompassing Central and North California, Oregon, and Washington.

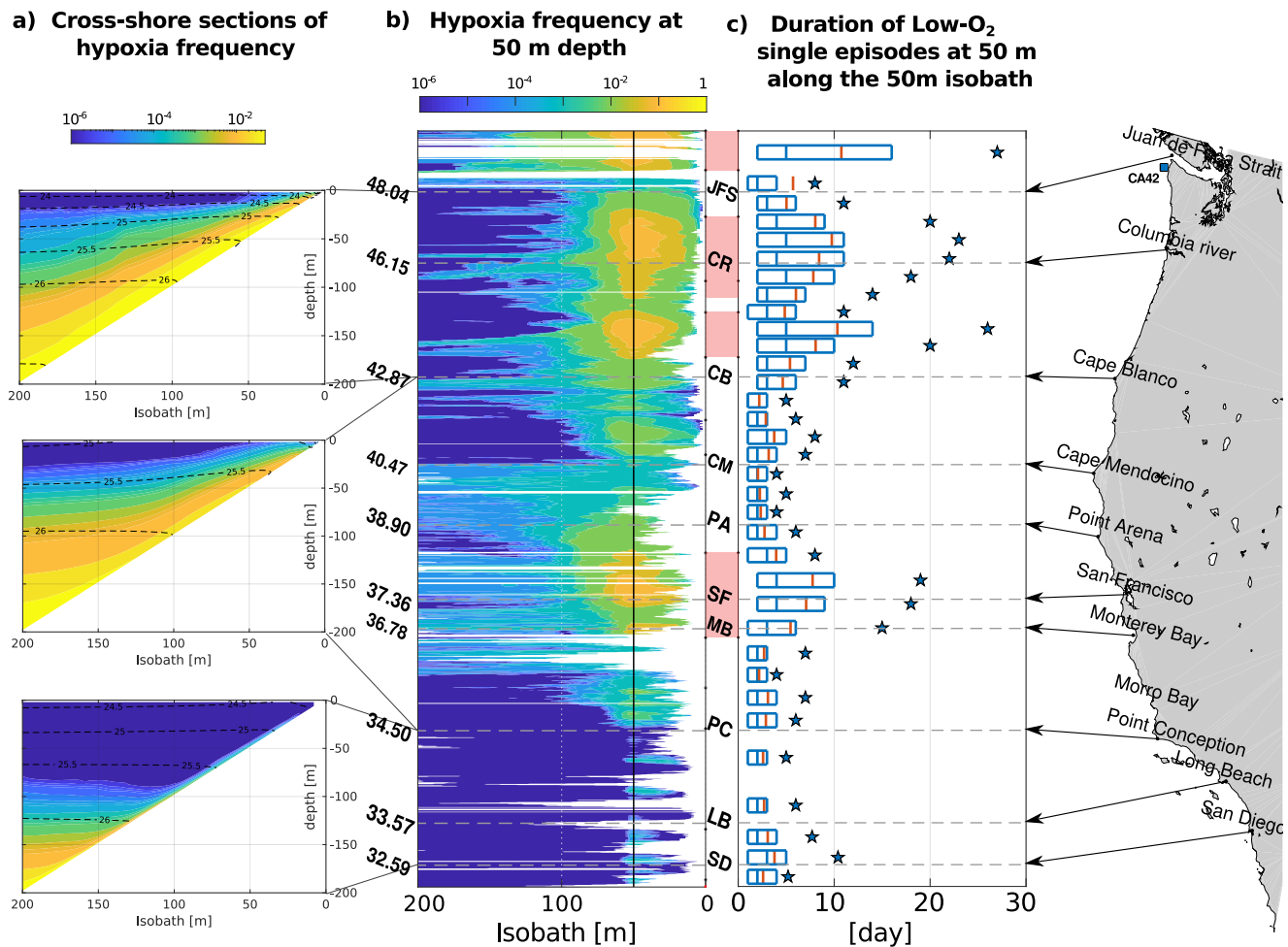


Figure 4. Frequency of hypoxic conditions and characteristics of hypoxic events on the U.S. West Coast continental shelf. (a) Cross sections of hypoxia frequency in year⁻¹ averaged over the shelves of three USWC regions. (b) Hypoxia frequency at 50 m depth with respect to the isobath. For waters shallower than 50 m, the hypoxia frequency at the bottom is shown. The white areas indicate locations where the corresponding isobath is absent due to the model resolution. (c) Statistics of hypoxic events with respect to latitude at 50 m depth along the 50 m isobath. This depth marks the shallowest point below the euphotic zone, indicating that OAH events at 50 m likely extend deeper, as shown in panel (a). Panel (b) highlights the peak occurrence at 50 m, making this isobath suitable for event duration statistics. The mean (red mark), 50th, 25th, 75th, and 90th percentiles (respectively blue central mark, the edges of the boxes and the stars) are represented in 0.5° zonal segments. The red shading blocks indicate alongshore hypoxia hotspots.

These patterns align with prior observations of recurrent hypoxia on the Heceta Bank (Adams et al., 2013, 2016; Connolly et al., 2010; Hales et al., 2006), the Washington State shelf (Barth et al., 2024; Connolly et al., 2010; Peterson et al., 2013), and central California (Chan et al., 2017), as well as pervasive shoaling of acidified waters on the USWC shelf (Feely et al., 2008, 2016).

On average along the USWC, the mean duration of individual extreme events is about 7 days for hypoxia and 15 days for acidification (Figures 4c and 5c). This is significantly shorter than seasonal timescales, indicating the importance of intra-seasonal variability (Connolly et al., 2010). For both hypoxia and acidification, the frequency and duration of individual events increase together from South to North. In general, the mean duration of events largely exceeds the median duration, indicating the presence of a small number of exceptionally long-lasting extremes. These outliers are particularly relevant for the marine biota because of the prolonged stress that they impose on marine organisms (Bednaršek et al., 2021; Gruber et al., 2021). The maximum event duration (shown by stars on Figures 4c and 5c) varies significantly along the coast, with a maximum duration of 27 days for hypoxia on the Heceta Bank, and 98 days for acidification on the Nehalem Bank. In California, particularly significant extreme events occur along the San Francisco to Monterey Bay coast, with a maximum duration of 19 and 37 days for hypoxia and acidification, respectively.

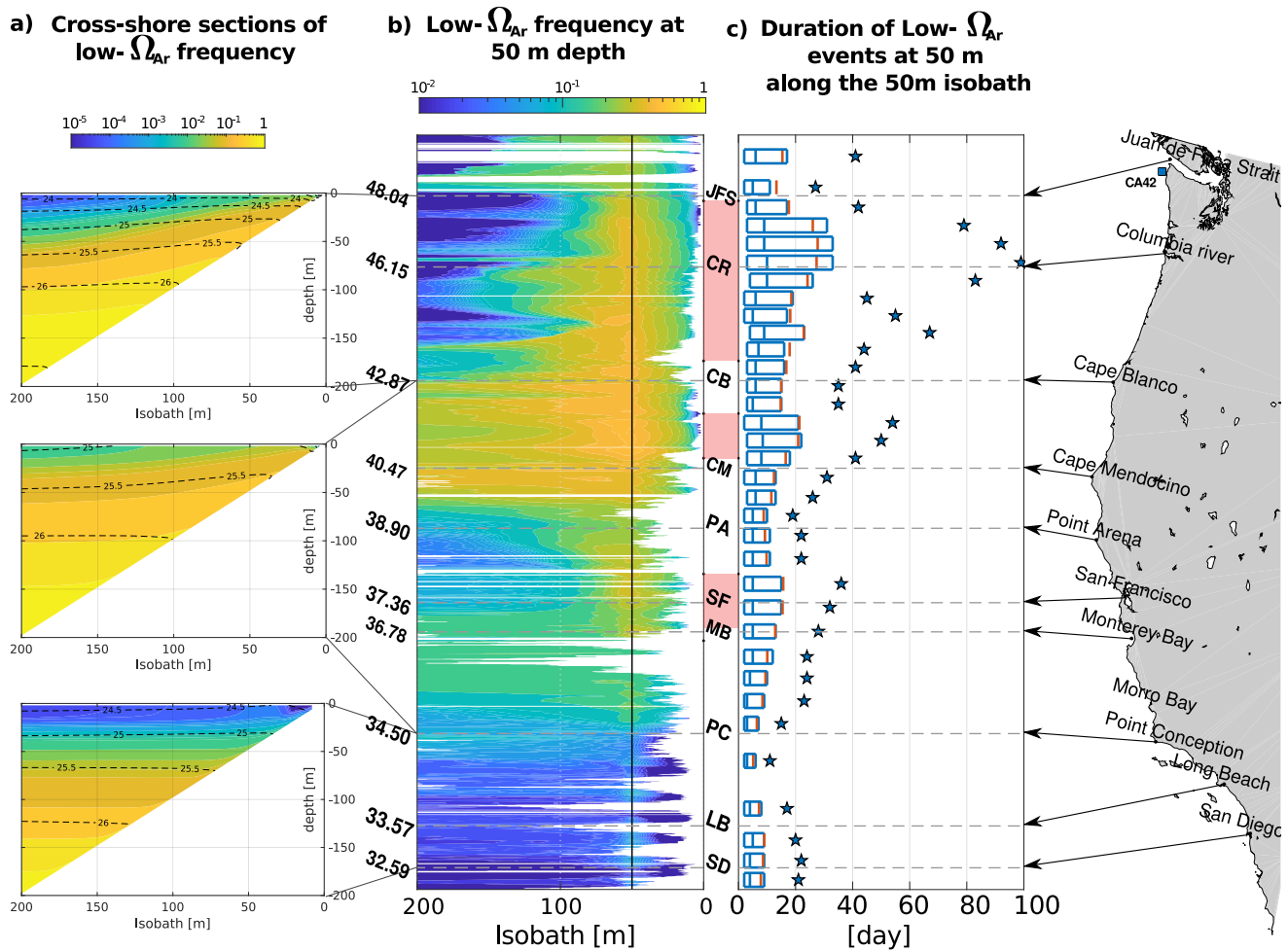


Figure 5. Frequency of ocean acidification conditions and characteristics of acidification events on the U.S. West Coast continental shelf. (a) Cross-sections of corrosive conditions frequency in year⁻¹ averaged over the shelves of three USWC regions. (b) Frequency of corrosive conditions at 50 m depth with respect to isobath. For waters shallower than 50 m, the frequency at the bottom is shown. The white areas indicate locations where the corresponding isobath is absent due to the model resolution. (c) Statistics of corrosive events with respect to latitude at 50 m depth along the 50 m isobath. The mean (red mark), 50th, 25th, 75th, and 90th percentiles (respectively blue central mark, the edges of the boxes and the stars) are represented in 0.5° zonal segments. The red shading blocks indicate the alongshore acidification hotspots.

Several mooring-based observational time series, including oxygen measurements, are available along the USWC. The coverage of moored assets predominantly favors the Washington and Oregon shelves, owing to two long-term programs maintained by the Olympic Coast National Marine Sanctuary (OCNMS, WA) and the Ocean Observatories Initiative (OOI, OR). The high frequency resolution of temperature and oxygen concentration at these mooring sites allows for a finer comparison against the simulation, targeted toward temporal variability, thereby toward a validation of the OAH events produced by the model. The time series of O₂ and Ω_{Ar} , computed from the empirical algorithm of Juraneck et al. (2009), are compared for the OCNMS station Cape Alava 42 (CA42) on the northern Washington shelf, and extreme events are reported in terms of number and duration (Figure 6). Similar comparisons at other stations are provided in Supporting Information S1 (Text S3, Figures S18–S31), and statistical metrics are used to evaluate the degree of agreement between the model time series and in situ observations (Tables T3–T5 in Supporting Information S1).

The model demonstrates an accurate representation of the seasonal cycle and sub-seasonal variability, as indicated by the similar amplitude of fluctuations during the upwelling season. The correlation coefficient between model and observations is 0.52 for O₂ and 0.69 for Ω_{Ar} (Table T3 in Supporting Information S1). We consider this agreement reasonable, considering that our model does not assimilate observations, and thus develops its own intrinsic variability (i.e., mesoscale and submesoscale eddies).

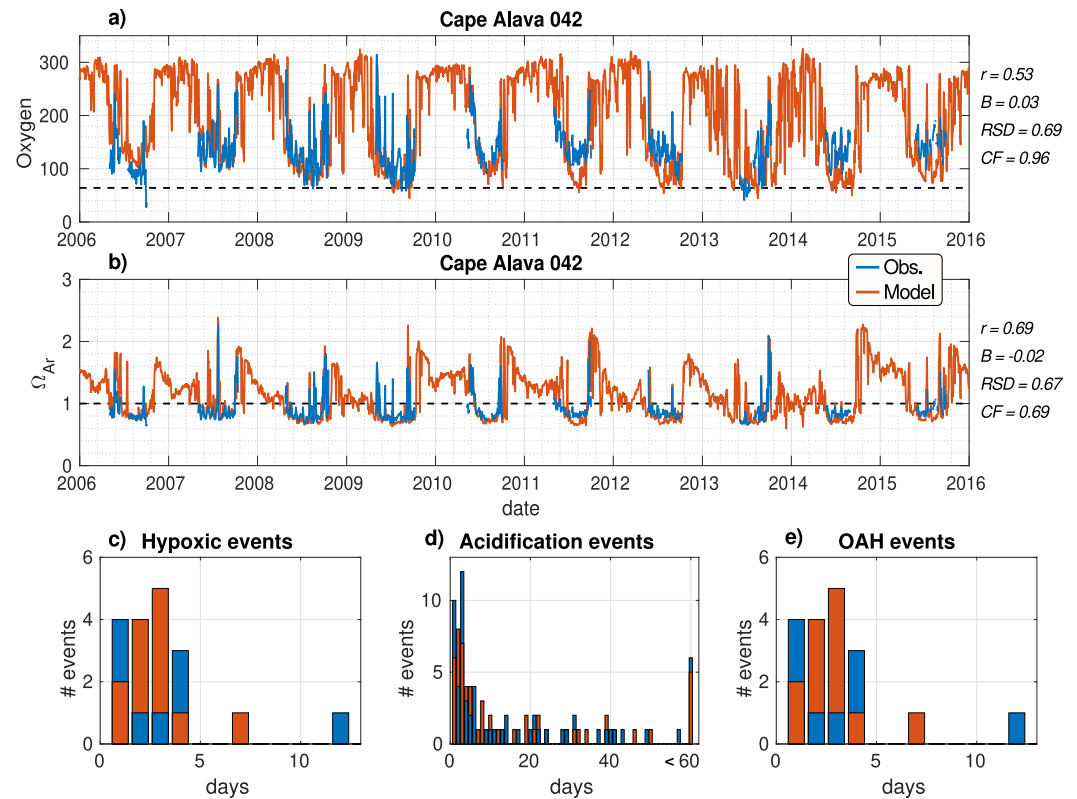


Figure 6. Time series of (a) O₂ concentration and (b) Ω_{Ar} at the bottom of the Olympic Coast National Marine Sanctuary station Cape Alava 42 (CA42) on the northern Washington shelf (location indicated on Figures 4 and 5), with observations shown by the blue line and model output by the red line. Metrics on the right statistically compare the numerical solution against observations, and consist of: the correlation coefficient (r) between the observations (D_n) and model time series (M_n); the bias ($B = \sum(D_n - M_n) / \sum D_n$) which measures the relative average difference between observations and the model; the ratio of the standard deviations (RSD), calculated as $RSD = \sigma_D / \sigma_M$, where σ is the standard deviation; and the cost function (CF), calculated as $CF = |D_n - M_n| / \sigma_D$, which evaluates the bias in the context of the variability associated with the observations. Further details on these metrics are provided in Text S2 in Supporting Information S1. Histograms of (c) hypoxic, (d) acidification, and (e) compound OAH events, with the duration of individual events (in days) on the x-axis and the number of events on the y-axis. Observations are shown in red, model output in blue. Simulated events are only reported when observations are available.

The model demonstrates strong overall performance in simulating extreme events. Similar to observations, it generates a large number of individual hypoxic events, typically lasting a few days, and acidification events with occurrences lasting more than 1 month. The statistical assessment of these events is comparable between model and observations. For example, the mean duration of observed and modeled hypoxic events is 3.3 and 2.8 days, respectively, while observed and modeled acidification events last 18.2 and 17.9 days. Further comparisons at different stations (Text S3 in Supporting Information S1) shows that the model successfully captures the variability observed across different stations.

From this model-based description of extreme events, several coastal regions emerge as more sensitive to the occurrence of either hypoxia or acidification. Applying a metric that combines both a local increase in occurrence and duration (see Section 2.2), we identify four hypoxia hotspots along the USWC (red boxes on Figure 4) the San Francisco shelf, the Heceta Bank, the Washington coast, and the Vancouver Island shelf. At these sites, hypoxic conditions may persist for over a month per year; for 25% of the events, the duration approaches or exceeds 1 week. Three regions emerge as prominent acidification hotspots (red boxes on Figure 5): the San Francisco shelf, Northern Cape Mendocino, and a large region extending from Heceta Bank to the Juan de Fuca Strait. Compared to hypoxia, acidification hotspots are characterized by more frequent and longer events, with a total duration greater than 3 months per year, and 25% of the events lasting longer than 16 days.

3.3. Compound Acidification and Hypoxic Events

The potential for hypoxia and acidification extreme events to occur simultaneously is high on the USWC, since both occur during the same season and are linked to upwelling and remineralization processes. Because the shelf is more frequently exposed to corrosive than hypoxic conditions (Figures 4 and 5), compound OAH extreme events are overall constrained by hypoxia in this region. Therefore, the occurrence, statistics, and regional hotspots of compound OAH events overlap nearly perfectly with those of hypoxic events. This is further demonstrated at station CA42, where the statistics of compound OAH events closely match those of hypoxic events (Figure 6).

The most extreme compound OAH conditions during the 20 years period are found in two subregions: the San Francisco shelf and the Northern USWC shelf (Figure 7a). At these hotspots, severe anoxia ($O_2 < 1 \text{ mmol m}^{-3}$) and Ω_{Ar} lower than 0.5 are encountered, with a wider surface area extension of acidic over hypoxic conditions. A detailed year-by-year examination of nearshore OAH compound events allows us to delineate the spatial extent of regions exposed every year (red line on Figure 7b). The occurrence of compound OAH events in these locations appears to be less sensitive to interannual variability, although climate variations may affect their severity. Compound OAH hotspots largely overlap with hypoxic hotspots across the coast, and include Monterey Bay, the San Francisco shelf, the Oregon and Washington shelves, and the western coast of Vancouver Island. In these regions, the accumulated time of exposure to compound OAH conditions is on average about 30 days each year.

Time series of O_2 and Ω_{Ar} reveal similarities in the variability of these properties over the course of the year, both in central California and in the northern USWC shelf (Figure 8). The seasonal OAH progression is punctuated by large subseasonal excursions, which play a fundamental role in the onset and termination of hypoxia and acidification events. Moreover, the large amplitude of subseasonal fluctuations in O_2 is critical for the occurrence of compounds OAH events (Figure 8c). The spatial extent of these events, largely defined by hypoxia (Figures 8a and 8b), also undergoes abrupt subseasonal fluctuations (Figure 8d). Together with the relatively low duration of individual OAH events (on the order of 2 weeks, Figure 4), the time series analysis shows that compound events in OAH hotspots are strongly constrained by large subseasonal fluctuations in O_2 and Ω_{Ar} . Coupled to the seasonal progression of OAH, these short-term fluctuations structure the frequency, duration, extent, and intensity of compound OAH events along the USWC.

3.4. Temporal Modes of Extreme Events Variability

Temporal variability at both seasonal and intraseasonal timescales contributes to the emergence of OAH events and hotspots along the USWC (Figure 9). In general, the variability (σ_{tot}) in O_2 and Ω_{Ar} tends to be anti-correlated with the mean of these quantities on the shelf (Figure 9). That is, areas with low average O_2 and Ω_{Ar} typically experience large fluctuations in these variables, making them prone to hypoxia or acidification exposure and preferential hotspots. This relationship is stronger for acidification than for hypoxia. As a consequence, hypoxic hotspots are not always overlapping with areas characterized by consistently low mean O_2 . For example, the mean O_2 concentrations on the shelf surrounding Point Arena tend to be low; in parallel, the O_2 variability (σ_{tot}) is also relatively low in this region, which is not classified as a hypoxia hotspot (Figures 9a and 9b).

The relative importance of seasonal (σ_{lf}) and sub-seasonal (σ_{hf}) fluctuations compared to total variability (σ_{tot}) differs significantly along the USWC, and as a function of depth (Figure 9). Low-frequency variations tend to dominate the total variability across the USWC, in particular on the deeper shelf, and are largely associated with the seasonal cycle of wind-driven upwelling. Variability at seasonal timescales shows large alongshore gradients, in particular near Cape Blanco. North of this location, a seasonal transition to downwelling favorable winds in winter expands the dynamical range of O_2 and Ω_{Ar} . Regions of more intense seasonal variability are well correlated with OAH hotspots along the USWC, confirming the central role of seasonal upwelling for the emergence of extreme events.

Variability on timescales shorter than a season (σ_{hf}) is far from negligible along the continental shelf (Adams et al., 2013, 2016; Connolly et al., 2010) (Figures 1 and 9) and is crucial for the establishment of OAH hotspots, especially south of Cape Blanco. In contrast to seasonal variability, high-frequency fluctuations are significantly larger on the upper shelf, where they account for nearly half of the total variability. This proportion increases to 80% between Cape Mendocino and Cape Blanco.

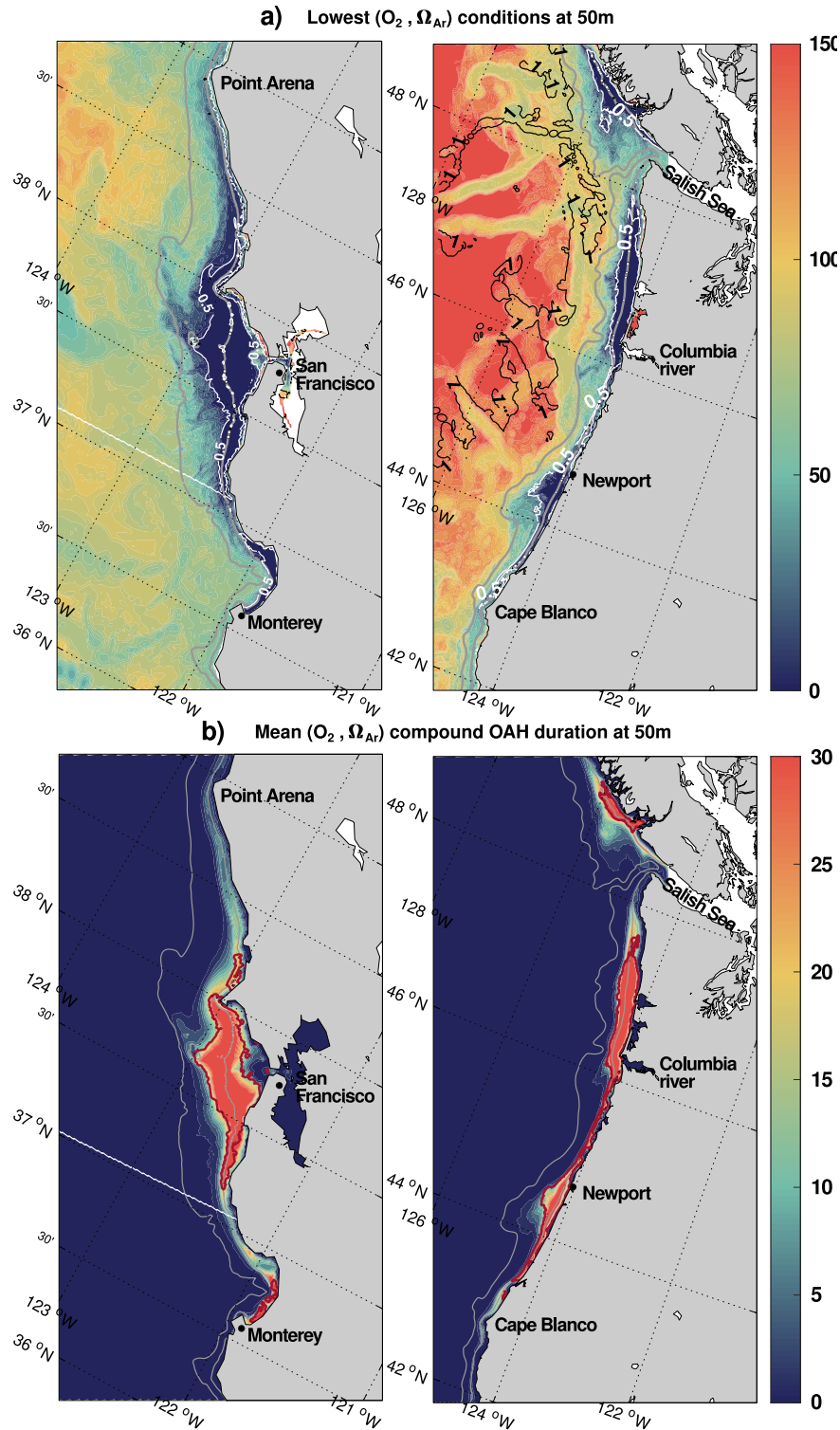


Figure 7. (a) Distribution of the lowest oxygen at 50 m depth (in mmol m^{-3}) for two USWC subregions in the 20-year-long model simulations. The lowest Ω_{Ar} at 50 m depth is superimposed (solid black contours for $\Omega_{Ar} = 1$ and solid white contours for $\Omega_{Ar} = 0.5$). On the left panel, the $\Omega_{Ar} = 1$ contour does not appear as $\Omega_{Ar} < 1$ everywhere. For waters shallower than 50 m depth, the minimum values in the bottom layer are shown (b). Cumulative duration of compound OAH ($\text{O}_2 < 64.0$ and $\Omega_{Ar} < 1$), expressed in days per year. The solid red contours indicate regions experiencing at least one compound OAH event per year during the 20 years of simulation. On all panels, solid gray contours show the 50 and 200 m isobaths.

3.5. Processes Controlling OAH at Seasonal Scale

As a necessary condition for OAH events to occur, we investigate the driving processes of the seasonal depletion of O_2 (Figure 10a) and Ω_{Ar} (Figure 11a) and their local modulations. Budgets are diagnosed with a focus on the region where OAH events frequently occur. They are vertically integrated below the euphotic layer where photosynthesis limits hypoxia development, with 50 m marking the average vertical limit of the euphotic layer in this region. The 100 m isobath is chosen for its position midway across the shelf width. This selection is supported by cross-sections of hypoxia occurrence (Figure 4a). Temporal variations in the onset and duration of OAH result from the combined effect of physical transport and biogeochemical transformations (Equation 3). Below the euphotic zone, remineralization of organic matter in the water column and in the sediment removes O_2 from seawater, while adding DIC (Sarmiento & Gruber, 2006), resulting in a net decline of Ω_{Ar} . The reduction in O_2 and Ω_{Ar} by remineralization varies significantly on seasonal scales (Figures 10c and 11c), and is largest in central California due to high primary production rates following upwelling (Damien, Bianchi, McWilliams, et al., 2023). Local regional variability is also noticeable, since alongshore spatial fluctuations exceed the amplitude of the seasonal cycle.

In contrast, physical transport fluctuates from negative contributions during winter and spring, to positive contributions during summer and fall (Figures 10b and 11b). The seasonal cycle in physical transport shows an alongshore transition between Cape Mendocino and Cape Blanco, north of which significantly larger negative contributions from transport are observed. The Monterey Bay and the shelf north of San Francisco exhibit a distinctive pattern of nearly year-round positive supply of O_2 by advection (Figure 10b), which partially offsets locally enhanced respiration rates.

In order to determine the mechanisms responsible for the seasonal subsurface reduction in O_2 and Ω_{Ar} , and highlight local variations, the terms of the governing equations are integrated in time over the period of seasonal decline to identify their respective contributions (Figures 10d and 11d). A focus on the seasonal decline period allows to diagnose the factors leading to the seasonal most severe conditions. Along the USWC, biogeochemical reactions, dominated by remineralization processes, are the main driver of this seasonal decrease. In Southern and Central California, remineralization is partially offset by physical supply. This is consistent with the prevailing paradigm, according to which hypoxia emerges due to an excess in respiration over physical O_2 supply (Fennel & Testa, 2019; Oschlies et al., 2018).

Along the Oregon and Washington shelves, a slightly distinct scenario unfolds, as physical depletion combines with respiration, and both cause seasonal oxygen loss and acidification. Remineralization remains the dominant driving force, while advection accounts for approximately 12% and 9% of the total O_2 and Ω_{Ar} seasonal decrease, respectively. Assuming that transport is mainly upwelling-driven during this season, this indicates that the source water has a lower oxygen concentration compared to shelf waters. The seasonal transport as a promoting factor for oxygen decline was suggested by Connolly et al. (2010) to explain an O_2 decline observed during summer 2006. They also noted that it was insufficient to induce hypoxia. Our seasonal O_2 budget aligns with the conclusions by Siedlecki et al. (2015), which identified respiration as the dominant driver of seasonal oxygen decline and highlighted the role of transport in exacerbating this decline. However, the relative magnitudes of these terms differ between our and their study. While Siedlecki et al. (2015) found that transport accounted for about 60% of the total respiration on the Washington coast, they also found that it was nearly negligible on the Oregon coast due to the retentive characteristics of the Heceta Bank. These discrepancies may be partly due to the different vertical layers considered in diagnosing the oxygen balance. Our analysis focuses on the bottom layer, where the transport term includes a vertical component from the surface oxygenated layer. We also exclude the subseasonal component, which is specifically addressed in the following section. For both O_2 and Ω_{Ar} , the shift to a negative net physical contribution occurs near the California-Oregon border.

Along the entire coastline, most O_2 consumption (65% on average) occurs in the sediment (Figure 10d). This is comparable to observational estimates (Connolly et al., 2010) that assign similar magnitudes to the two processes.

Seasonal acidification is mostly the consequence of subsurface DIC release by remineralization, which is only marginally offset by alkalinity production. On average, release of alkalinity by remineralization and dissolution of calcium carbonate counterbalances the decline in Ω_{Ar} caused by the release of DIC by 8.2%, with a maximum north of Cape Mendocino (14.7%). The increasing contribution of alkalinity to the decline in Ω_{Ar} in this region aligns with results from Hauri, Gruber, Vogt, et al. (2013), although it is somewhat weaker in our model.

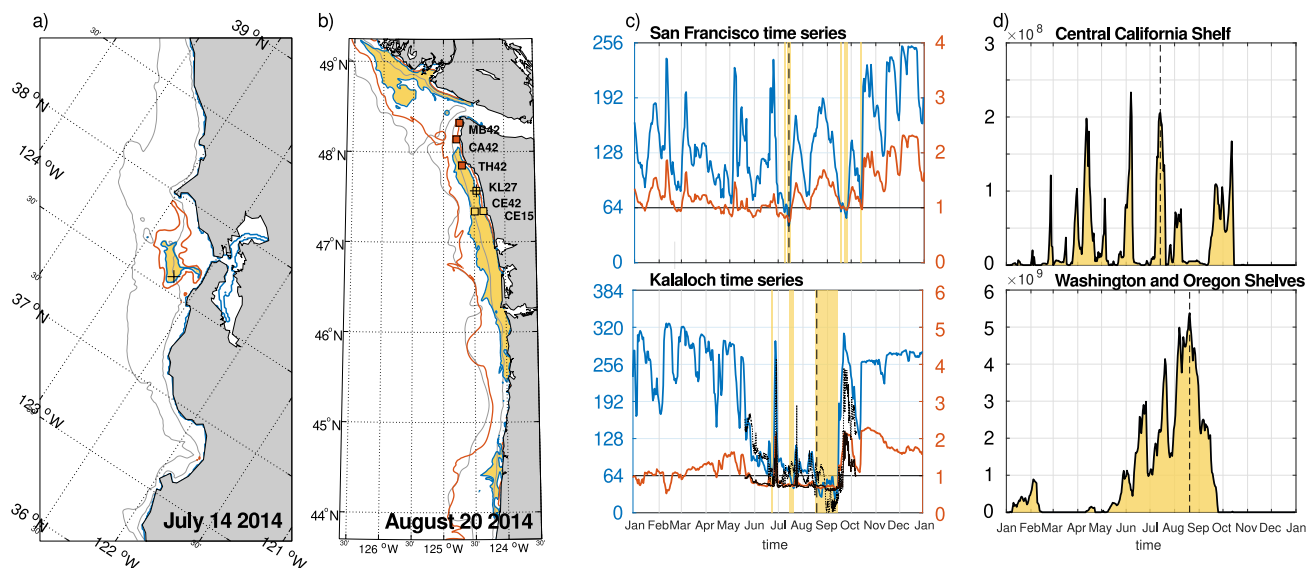


Figure 8. Instantaneous extent of hypoxia (blue) and acidification (red) on (a) the Central California shelf, and (b) the Oregon-Washington shelf. The extent is shown at 50 m and at the bottom for waters shallower than 50 m. Gray contours indicate the 50 and 200 m isobaths. The yellow shadings highlight the extent of OAH compound conditions. Panels (a) and (b) show two different days during summer 2014: July 14 and August 20, respectively. This year was chosen because observations from several OCNMS moorings were available simultaneously on the Washington shelf. Their locations are shown by square markers in panel (b) and are labeled by name. Stations that experienced an acidification event during the week centered on 20 August 2014, are colored in red. Stations that experienced a compound OAH event during the same period are colored in yellow. (c) Time-series of O_2 (blue, mmol m^{-3}) and Ω_{Ar} (red, non-dimensional) at 50 m depth on (upper panel) the San Francisco and (lower panel) Washington shelves. Exact locations are shown by black crosses on the maps in (a) and (b). The OCNMS Kalaloch 27 station (KL27) is chosen on the Washington shelf to compare with the measurements from the moored asset. The observed time series are plotted as thin black lines, with O_2 represented by a dashed line and Ω_{Ar} by a solid line. Yellow shaded boxes highlight periods of OAH compound events. (d) Time-series of the compound OAH surface area extent (in km^2) in the Central California shelf (upper panel), and in the Oregon-Washington Shelf (lower panel). This area is defined at 50 m and the bottom depth is considered for waters shallower than 50 m.

In Northern and Central California, local OAH hotspots are associated with locally enhanced seasonal remineralization. This spatial variability is mostly caused by alongshore changes in the strength of upwelling and the resulting primary production. Here, the seasonal depletion in O_2 and Ω_{Ar} is only partially offset by physical transport. Enhanced subsurface respiration appears to be a necessary but not sufficient condition for the occurrence of OAH hotspots. For example, the region between Point Arena and Cape Mendocino, which shows a local peak in remineralization rates, is not an OAH hotspot. This is likely due to the relatively weak high-frequency variability (σ_{hf}) in O_2 and Ω_{Ar} (Figure 9), which inhibits the onset of OAH conditions.

In both the Southern California Bight and the Oregon-Washington shelves, OAH hotspots are not necessarily characterized by locally intensified remineralization rates. Overlap between these hotspots and regions characterized by large seasonal variations is also weak. This suggests an increasingly important role for sub-seasonal variability in triggering OAH events.

3.6. Effect of High-Frequency Fluctuations

We investigate the effect of short-term fluctuations on the statistics of OAH events during year 2001, which was selected due to the absence of strong interannual signals (Figure 12). High frequency variations in physical fluxes and biogeochemical rates significantly increase the overall duration of OAH conditions but also produce shorter individual events (Figures 12a and 12b). The impact of short term fluctuations on the cumulative duration is particularly important for hypoxia, which increases by a factor of 3.1 in the Monterey-San Francisco hotspot, and by a factor of 5.2 on the Oregon-Washington shelf. Equally important, the duration of individual OAH events decreases on average by a factor of 5.4 when sub-seasonal fluctuations are considered. This reduction factor is larger for acidification events, which are shortened by up to 10-fold along the Oregon and Washington shelves. The intensity of extreme events, diagnosed by the O_2 concentration and Ω_{Ar} reached during the year (Figure 12c), is larger when short-term fluctuations are considered. This effect is large: on average, high frequency fluctuations reduce O_2 by 43.7 mmol m^{-3} during hypoxic events, and Ω_{Ar} by 0.28 units during acidification events.

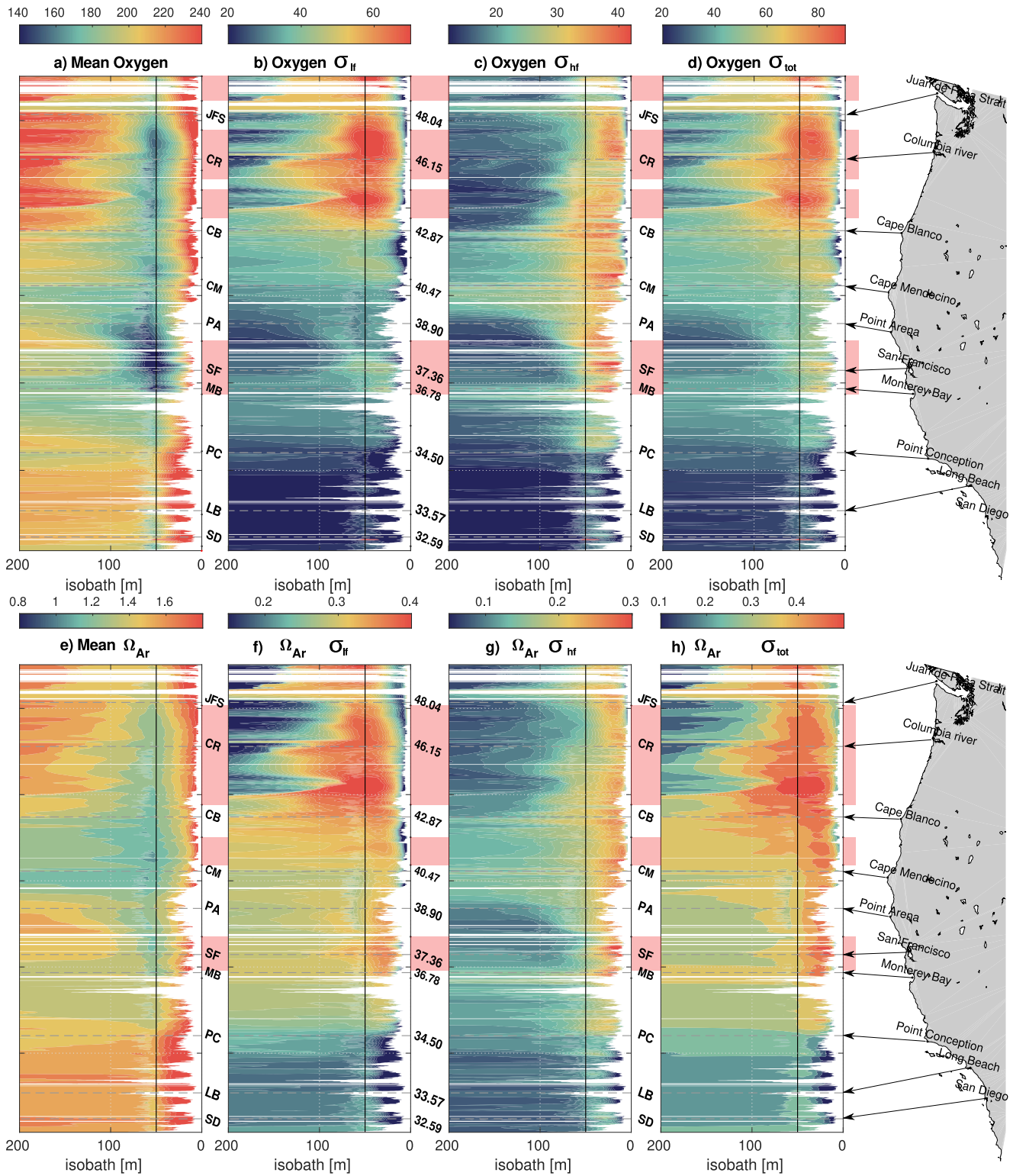


Figure 9. Mean state and variability in O_2 (upper panels in mmol m^{-3}) and Ω_{Ar} (lower panels) on the U.S. West coast shelf: (a, e) Mean state, (b, f) seasonal variance, (c, g) sub-seasonal variance, and (d, h) total variance. Fields are shown at 50 m depth and at the bottom for waters shallower than 50 m. The red shaded boxes next to each panel highlight alongshore OAH hotspots.

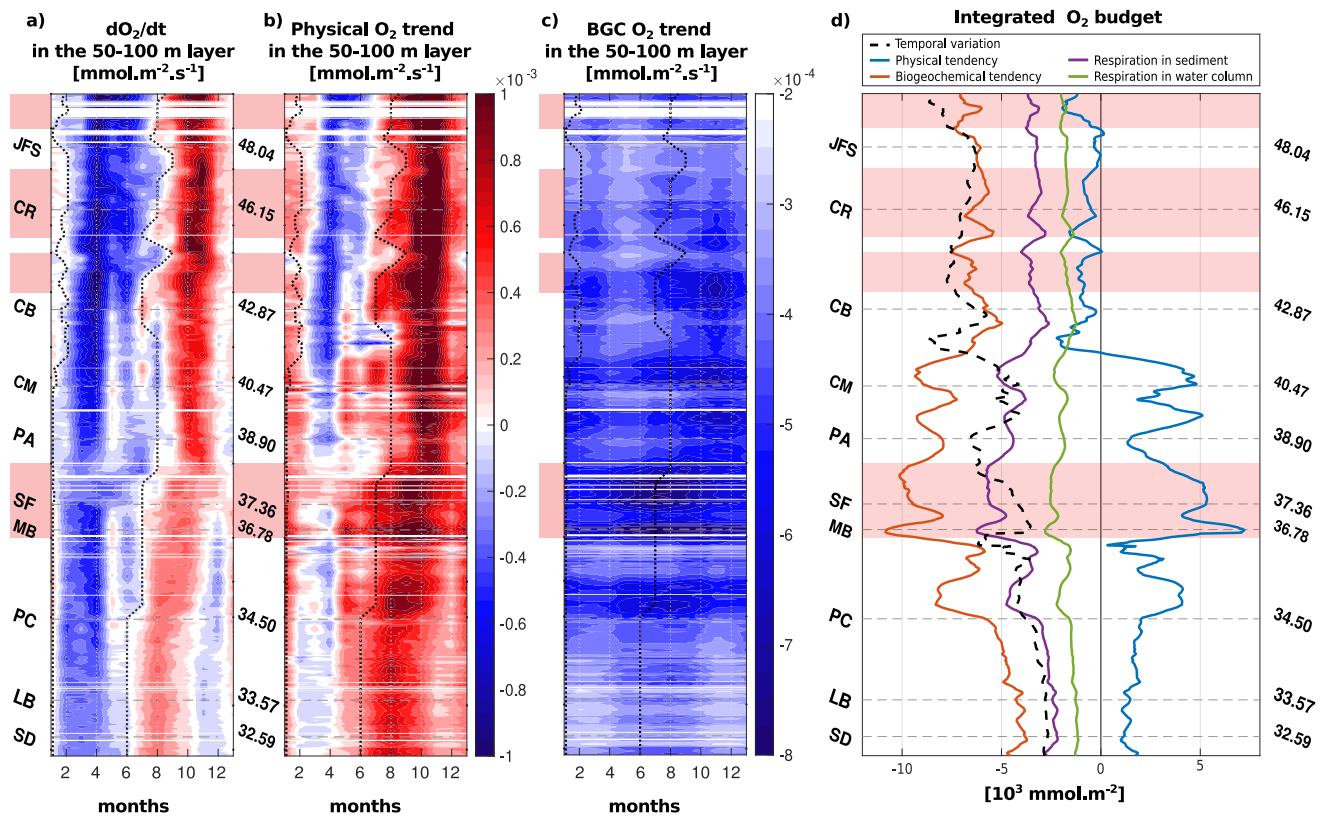


Figure 10. Seasonal oxygen tendency and drivers below the surface along the 100 m isobath. Panels (a–c) show, respectively, the monthly rate of change in oxygen, the physical and the biogeochemical oxygen tendencies, integrated across the 50–100 m layer below the euphotic layer. The dashed black lines show the monthly maximum and minimum O_2 levels, bracketing the period of seasonal O_2 decrease. Panel (d) shows the oxygen balance integrated over the seasonal O_2 decrease period. The oxygen temporal variation (dashed black line) results from the sum of the physical term (blue) and the biogeochemical term (red). Respiration in the sediment (purple) and the water column (green) are also shown as the dominant components of the biogeochemical rates. The red shaded boxes highlight alongshore hypoxia hotspots.

To summarize, short-term fluctuations play three important roles on the characteristics of OAH events. First, they facilitate the event onset by exacerbating the effect of seasonal drivers. This is demonstrated by the longer cumulative OAH period when short-term fluctuations are considered. Second, they produce more intense events, as shown by the lower values reached by O_{2tot} and Ω_{Artot} compared to the low-frequency equivalent. Third, and in contrast with the previous influences, short-term fluctuations generate individual OAH events with a shorter duration on average. This provides relaxation periods that increase the number of individual events, but decrease their average duration. As a consequence, the influence of short-term fluctuations is twofold, as they significantly increase the frequency and severity of extreme events, but also lead to shorter individual events.

Mechanistically, Figure 13a demonstrates a close correspondence between temporal variation and transport at high frequency, suggesting that intra-seasonal fluctuations in O_2 and Ω_{Ar} are primarily driven by the physical transport terms of the respective balance equations. On daily time scales, the rate of change in O_2 (dO_2/dt) can reach up to $140 mmol m^{-3} d^{-1}$, and the rate of change in Ω_{Ar} ($d\Omega_{Ar}/dt$) up to $1.4 d^{-1}$. This is larger than, but not inconsistent with, daily oxygen variations observed on the Oregon-Washington continental shelf (Connolly et al., 2010). Regardless of their signs, these transports are large enough to initiate or terminate an extreme event within a few days, considering that O_2 and Ω_{Ar} are close to the extreme event thresholds. High frequency physical fluctuations in both O_2 and Ω_{Ar} ($PHY'(O_2)$ and $PHY'(\Omega_{Ar})$) exhibit larger positive values, that is, they tend to increase O_2 and Ω_{Ar} . Put it differently, the probability distributions of the high frequency physical transport terms are positively skewed. This supports the result that high frequency physical fluctuations can provide relaxation periods by breaking longer OAH intervals into shorter events.

For both O_2 and Ω_{Ar} , short-term fluctuations in physical transport are significantly correlated with the alongshore wind stress and wind stress curl (Figures 13b and 13c). This indicates that intra-seasonal O_2 and Ω_{Ar} variations are

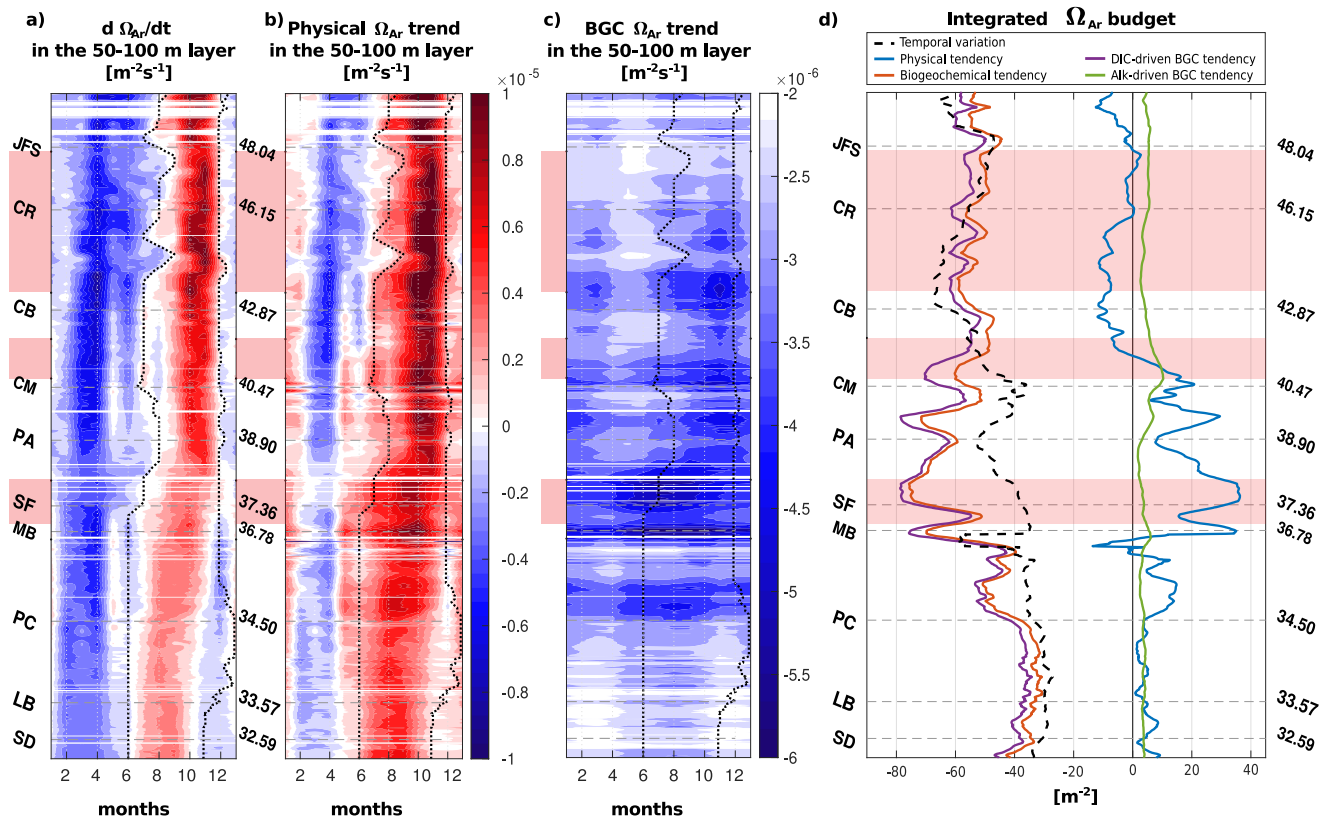


Figure 11. (a, b, and c) Same as Figure 10, but for the seasonal balance of subsurface Ω_{Ar} . In panel (d), the temporal variation (dashed black line) results from the sum of the physical term (blue) and the biogeochemical term (red). The latter is further decomposed into its DIC (purple) and alkalinity (green) components.

mostly forced by winds. We speculate that brief episodes of alongshore wind intensification, relaxation, or direction reversal during upwelling-favorable conditions may play an important role in mitigating the effects of OAH. A similar role for brief wind events on the concentration of oxygen and particulate organic carbon was observed over the Heceta Bank by Hales et al. (2006). However, the relationship between wind and transport is not entirely consistent, illustrating that short-term fluctuations in transport are not completely determined by winds. In addition to wind-driven transport, submesoscale variability is known to significantly modulate transport and hence might also play a secondary role.

4. Discussion and Conclusions

Our analysis of two 20-year long simulations with a submesoscale permitting physical-biogeochemical model reveals the emergence of hypoxia and acidification hotspots in the CCS. These hotspots are particularly pronounced in regions such as the San Francisco shelf in Central California, and the northern Oregon-Washington shelf. This spatial description of sensitive areas aligns with previous studies (Chan et al., 2008; Feely et al., 2024; Siedlecki et al., 2015), and further highlights their limited sensitivity to interannual variability, as extreme events occur consistently from year to year during the simulated period. The co-occurrence of acidification and hypoxia, or compound OAH events (Gruber et al., 2021), is predominantly constrained by hypoxia because of the more pervasive exposure of the USWC to ocean acidification. The good correlation along the coast between hypoxia and shelf width can be further attributed to the retentive characteristics of wider banks, which exhibit longer residence times relative to narrower banks (Hickey & Banas, 2008; Siedlecki et al., 2015). Our analysis provides a statistical characterization of OAH hotspots and characterizes areas along the coast where OAH conditions are comparatively less severe (Chan et al., 2017). These areas may represent potential ecological refuges from the dual threats of global acidification and oxygen loss. In this context, our study highlights regional vulnerabilities and potentially important areas for ecosystem management efforts.

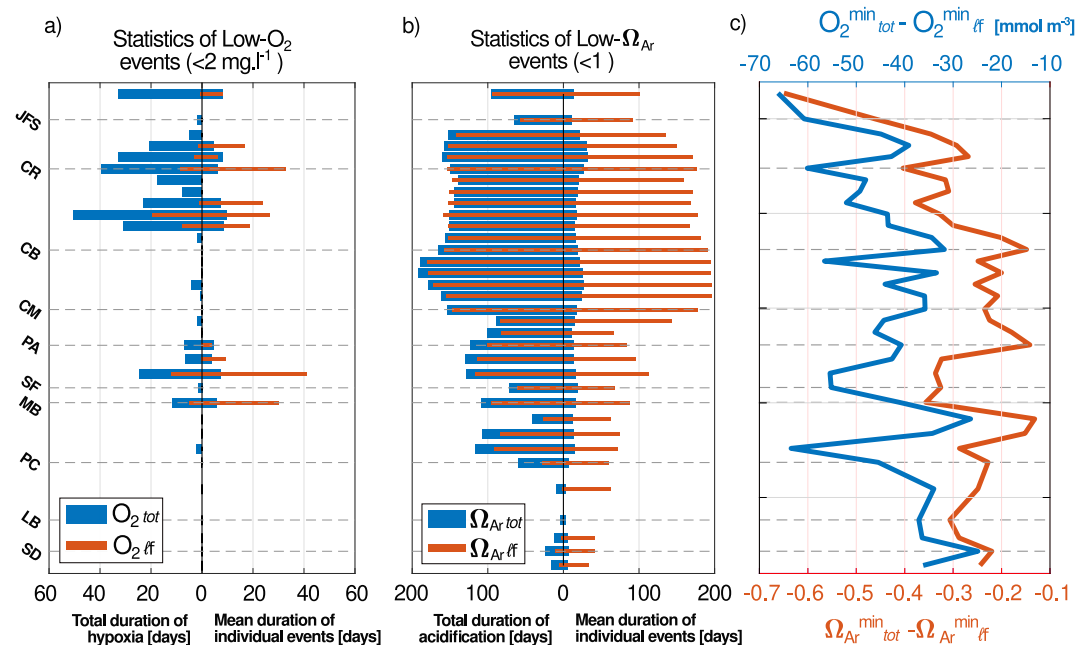


Figure 12. Cumulative duration of (a) hypoxic and (b) acidified conditions expressed in days per alongshore distance in km (left-side of the panels) and mean duration of individual events in days (right-side of the panels). These quantities are calculated for 0.5° alongshore transects during year 2001 based on high frequency time series of O_2 and Ω_{Ar} (blue), labeled by the “tot” subscript, and low frequency O_2 and Ω_{Ar} time series (red), labeled by the “lf” subscript, obtained by high-pass filtering of the respective conservation equations (see Section 2.4 and Equations 7 and 8). (c) Illustration of OAH extremes induced by high-frequency physical and biogeochemical contributions, here encapsulated by the difference between the lowest O_2 and Ω_{Ar} values in the high frequency minus the low frequency time series. All panels are based on variables extracted along the 50 m isobath at the bottom.

Along the USWC, the onset and termination of OAH events involve a combination of physical and biogeochemical processes operating across a range of temporal scales. At seasonal scales, remineralization in the water column and sediment predominantly drives the seasonal decline in oxygen and aragonite saturation. In contrast, while transport mitigates these decreases in Southern and Central California, it promotes them along the Northern coast. This result aligns with the conclusions of previous studies that diagnosed the O_2 budget on the Oregon and Washington shelves (Connolly et al., 2010; Siedlecki et al., 2015), although differences in the relative magnitudes can be partly attributed to different methodologies. In our study, we further identify the region near the California-Oregon border as a transition for the relative net contribution of transport to the seasonal O_2 and Ω_{Ar} decrease.

These regional differences suggest potential distinct responses to long-term changes such as decadal climate variability and anthropogenic change, with varied ecological implications. For example, recurrent observations of hypoxia have been reported since 2000 in the northern USWC, while little prior evidence (Barth et al., 2024; Chan et al., 2008). By demonstrating that transport processes favors seasonal oxygen depletion in the northern USWC, our study suggests that emerging hypoxia may result from the on-shelf advection of waters masses with progressively lower oxygen content. Aligned with this hypothesis, previous studies propose a combination of shifting properties of source waters (Bograd et al., 2008; Connolly et al., 2010; Evans et al., 2020), and a deeper origin of upwelled waters under shifting climatic conditions (Deutsch et al., 2014) to explain observed declines. More generally, understanding regional particularities is crucial to refine future predictions and to tailor conservation efforts and ecosystem management to specific areas.

A novel aspect of our study lies in the exploration of short-term fluctuations and their profound impact on OAH events and extremes. High frequency variability appears crucial to model realistic OAH extremes lasting for a few days that compare well with observed OAH events (Adams et al., 2016; Connolly et al., 2010; Harris et al., 2013). The comparison of physical transport and wind fluctuations suggests that wind is a dominant driver of abrupt changes in OAH events. Our findings reveal that subseasonal variability, dominantly due to physical transport, significantly increases the occurrence of OAH events and intensifies their severity but also leads to shorter

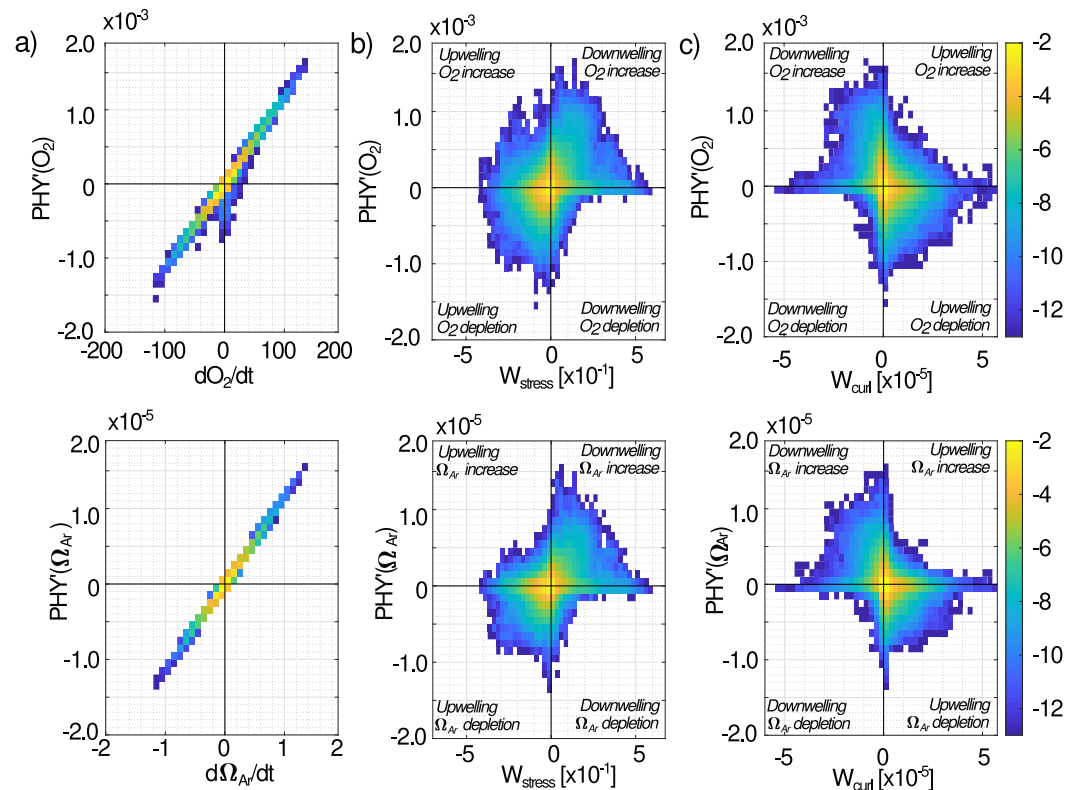


Figure 13. Role of short-term fluctuations in the physical transport terms for O_2 (upper panels) and Ω_{Ar} (lower panels) and relationship with wind forcings. All panels show the normalized joint probability density of high-frequency fluctuations in physical transport, $PHY'(O_2)$ and $PHY'(\Omega_{Ar})$, versus (a) the daily temporal rate of change in O_2 and Ω_{Ar} , (b) the daily alongshore wind stress (positive northward), and (c) the wind stress curl. Color contours show joint probability densities on a logarithmic scale, so that the distributions sum to one over the respective domains. All panels are based on values taken along the 50 m isobath at the bottom. dO_2/dt is in units of $mmol\ m^{-3}\ d^{-1}$, $d\Omega_{Ar}/dt$ in d^{-1} , W_{stress} in $N\ m^{-2}$, W_{curl} in $N\ m^{-1}$, $PHY'(O_2)$ in $mmol\ m^{-3}\ s^{-1}$ and $PHY'(\Omega_{Ar})$ in s^{-1} . The four quadrants in panels (b) and (c) represent scenarios of positive/negative wind stress and curl, corresponding to upwelling/downwelling favorable conditions, respectively, combined with an increase/decrease due to physical transport. These scenarios are labeled in each quadrant.

individual events. The resulting impacts on marine organisms are challenging to predict, since high-frequency fluctuations exacerbate potentially harmful conditions but also cause relaxation periods that may favor ecosystem resilience during the OAH-favorable upwelling season.

Beyond seasonal and intraseasonal fluctuations, the CCS is also affected by interannual to multi-decadal variability (Franco et al., 2023; Jacox et al., 2014; Peterson et al., 2013; Turi et al., 2016), superimposed to the secular trends of oxygen loss and acidification caused by anthropogenic climate change (Orr et al., 2005; Pierce et al., 2012). This low-frequency variability influences the occurrence and intensity of extreme events from year to year (Cheresh et al., 2023). Although our simulation shows significant coast-wide acidification and oxygen loss trends between 1997 and 2017 (see time series in Figures S6–S16 in Supporting Information S1), these trends are non-linear, are strongly modulated by climate variability on decadal time scales, and vary significantly along the coast. Their significance is then questionable considering the difficulty to distinguish between decadal variations and long-term forced trends in a 20-year time series (Crawford & Peña, 2016). As a result, our analysis does not encompass low-frequency signals, although these are likely to influence the distribution, frequency and intensity of OAH hotspots across the USWC.

There are limitation to our study that should be addressed by future work. We do not explicitly address the role of terrestrial nutrient inputs from rivers (Davis et al., 2014) and wastewater outfalls. Kessouri, McWilliams, et al. (2021) show that the inclusion of ocean outfalls leads to a seasonal reductions in subsurface O_2 by up to $50\ mmol\ m^{-3}$ and Ω_{Ar} by up to 0.47 in the Southern California Bight. Given the magnitude of this anthropogenic impact, it is likely that such changes could contribute to the emergence OAH events in this region. The lack of

nutrient inputs from rivers and point sources likely results in an underestimate of OAH risk, particularly in regions that are strongly affected by river runoff and human activities, such as the Gulf of Farallones outside the San Francisco Bay, Monterey Bay, and the Southern California Bight. In addition, the lack of tides and waves may limit variability in our simulations (Adams et al., 2013; Frieder et al., 2012). Further modeling work should explore the role of coastal eutrophication and higher frequency (e.g., sub-inertial) circulations. We also used specific, constant thresholds to define OAH conditions. Future analysis of the biological impacts of OAH should consider variable and organism-dependent thresholds (Bednaršek et al., 2021; Howard et al., 2020), and the regional and temporal adaptive capacity of species and ecosystems.

Data Availability Statement

The model code used to generate the simulation is openly available in Kessouri, McWilliams, Deutsch, et al. (2020) (<https://doi.org/10.5281/zenodo.3988618>). The simulations are reproducible using the setup and forcing described in Damien, Bianchi, McWilliams, et al. (2023). The mooring-based time series from the stations maintained by OCNMS (WA) are accessible online (<https://olympiccoast.noaa.gov/science/oceanographic-moorings/data.html>). Observations from the CalCOFI program can be found on their website (<https://calcofi.org>). SMBO observations are on the SCOOS data portal (<https://data.caloos.org/>); and SPOT are accessible on a dedicated website: <https://dornsife.usc.edu/spot/data-archive/>. The NOAA makes available the data from West Coast Ocean Acidification Cruises (WCOA) through OCADS (<https://www.ncei.noaa.gov/access/ocean-carbon-acidification-data-system/oceans/Coastal/WCOA.html>) and the World Ocean Database through (<https://www.ncei.noaa.gov/products/world-ocean-database>).

Acknowledgments

This work was supported by NSF Grants OCE-1847687 and OCE-1419323, NOAA Grants NA15NOS4780186 and NA18NOS4780174, California Ocean Protection Council Grants C0100400 and C0831014, and ARPA-E Grant DE-AR0001559. This work used the Expanse system at the San Diego Supercomputer Center through allocation TG-OCE170017 from the Advanced Cyber infrastructure Coordination Ecosystem: Services and Support (ACCESS) program, which is supported by National Science Foundation Grants 2138259, 2138286, 2138307, 2137603, and 2138296.

References

- Adams, K. A., Barth, J. A., & Chan, F. (2013). Temporal variability of near-bottom dissolved oxygen during upwelling off central Oregon. *Journal of Geophysical Research: Oceans*, 118(10), 4839–4854. <https://doi.org/10.1002/jgrc.20361>
- Adams, K. A., Barth, J. A., & Shearman, R. K. (2016). Intraseasonal cross-shelf variability of hypoxia along the Newport, Oregon, hydrographic line. *Journal of Physical Oceanography*, 46(7), 2219–2238. <https://doi.org/10.1175/jpo-d-15-0119.1>
- Alin, S. R., Feely, R. A., Dickson, A. G., Hernández-Ayón, J. M., Juranek, L. W., Ohman, M. D., & Goericke, R. (2012). Robust empirical relationships for estimating the carbonate system in the southern California current system and application to calcofi hydrographic cruise data (2005–2011). *Journal of Geophysical Research*, 117(C5). <https://doi.org/10.1029/2011JC007511>
- Barth, J. A., Pierce, S. D., Carter, B. R., Chan, F., Erofeev, A. Y., Fisher, J. L., et al. (2024). Widespread and increasing near-bottom hypoxia in the coastal ocean off the United States Pacific northwest. *Scientific Reports*, 14(1), 3798. <https://doi.org/10.1038/s41598-024-54476-0>
- Bednaršek, N., Ambrose, R., Calosi, P., Childers, R. K., Feely, R. A., Litvin, S. Y., et al. (2021). Synthesis of thresholds of ocean acidification impacts on decapods. *Frontiers in Marine Science*, 8, 651102. <https://doi.org/10.3389/fmars.2021.651102>
- Bednaršek, N., Feely, R. A., Howes, E. L., Hunt, B. P., Kessouri, F., León, P., et al. (2019). Systematic review and meta-analysis toward synthesis of thresholds of ocean acidification impacts on calcifying pteropods and interactions with warming. *Frontiers in Marine Science*, 6, 227. <https://doi.org/10.3389/fmars.2019.00227>
- Bednaršek, N., Feely, R. A., Reum, J. C., Peterson, B., Menkel, J., Alin, S. R., & Hales, B. (2014). *Limacina helicina* shell dissolution as an indicator of declining habitat suitability owing to ocean acidification in the California current ecosystem. *Proceedings of the Royal Society B: Biological Sciences*, 281(1785), 20140123. <https://doi.org/10.1098/rspb.2014.0123>
- Bednaršek, N., Feely, R. A., Tolimieri, N., Hermann, A., Siedlecki, S., Waldbusser, G., et al. (2017). Exposure history determines pteropod vulnerability to ocean acidification along the US west coast. *Scientific Reports*, 7(1), 4526. <https://doi.org/10.1038/s41598-017-03934-z>
- Bednaršek, N., Harvey, C. J., Kaplan, I. C., Feely, R. A., & Možina, J. (2016). Pteropods on the edge: Cumulative effects of ocean acidification, warming, and deoxygenation. *Progress in Oceanography*, 145, 1–24. <https://doi.org/10.1016/j.pocean.2016.04.002>
- Bednaršek, N., & Ohman, M. (2015). Changes in pteropod distributions and shell dissolution across a frontal system in the California current system. *Marine Ecology Progress Series*, 523, 93–103. <https://doi.org/10.3354/meps11199>
- Bograd, S. J., Castro, C. G., Di Lorenzo, E., Palacios, D. M., Bailey, H., Gilly, W., & Chavez, F. P. (2008). Oxygen declines and the shoaling of the hypoxic boundary in the California current. *Geophysical Research Letters*, 35(12). <https://doi.org/10.1029/2008gl034185>
- Booth, J. A. T., McPhee-Shaw, E. E., Chua, P., Kingsley, E., Denny, M., Phillips, R., et al. (2012). Natural intrusions of hypoxic, low pH water into nearshore marine environments on the California coast. *Continental Shelf Research*, 45, 108–115. <https://doi.org/10.1016/j.csr.2012.06.009>
- Breitburg, D., Levin, L. A., Oschlies, A., Grégoire, M., Chavez, F. P., Conley, D. J., et al. (2018). Declining oxygen in the global ocean and coastal waters. *Science*, 359(6371), eaam7240. <https://doi.org/10.1126/science.aam7240>
- Burger, F. A., John, J. G., & Frölicher, T. L. (2020). Increase in ocean acidity variability and extremes under increasing atmospheric CO₂. *Biogeosciences*, 17(18), 4633–4662. <https://doi.org/10.5194/bg-17-4633-2020>
- Cai, W.-J., Hu, X., Huang, W.-J., Murrell, M. C., Lehrter, J. C., Lohrenz, S. E., et al. (2011). Acidification of subsurface coastal waters enhanced by eutrophication. *Nature Geoscience*, 4(11), 766–770. <https://doi.org/10.1038/ngeo1297>
- Capet, X., McWilliams, J. C., Molemaker, M. J., & Shchepetkin, A. F. (2008). Mesoscale to submesoscale transition in the California Current System. Part I: Flow structure, eddy flux, and observational tests. *Journal of Physical Oceanography*, 38(1), 29–43. <https://doi.org/10.1175/2007jpo3671.1>
- Chan, F., Barth, J., Blanchette, C., Byrne, R., Chavez, F., Cheriton, O., et al. (2017). Persistent spatial structuring of coastal ocean acidification in the California current system. *Scientific Reports*, 7(1), 2526. <https://doi.org/10.1038/s41598-017-02777-y>
- Chan, F., Barth, J., Lubchenco, J., Kirincich, A., Weeks, H., Peterson, W. T., & Menge, B. (2008). Emergence of anoxia in the California current large marine ecosystem. *Science*, 319(5865), 920. <https://doi.org/10.1126/science.1149016>

- Cheresh, J., & Fiechter, J. (2020). Physical and biogeochemical drivers of alongshore pH and oxygen variability in the California current system. *Geophysical Research Letters*, *47*(19), e2020GL089553. <https://doi.org/10.1029/2020gl089553>
- Cheresh, J., Kroeker, K. J., & Fiechter, J. (2023). Upwelling intensity and source water properties drive high interannual variability of corrosive events in the California current. *Scientific Reports*, *13*(1), 13013. <https://doi.org/10.1038/s41598-023-39691-5>
- Connolly, T. P., Hickey, B. M., Geier, S. L., & Cochlan, W. P. (2010). Processes influencing seasonal hypoxia in the northern California current system. *Journal of Geophysical Research*, *115*(C3). <https://doi.org/10.1029/2009jc005283>
- Crawford, W. R., & Peña, M. A. (2016). Decadal trends in oxygen concentration in subsurface waters of the northeast Pacific Ocean. *Atmosphere-Ocean*, *54*(2), 171–192. <https://doi.org/10.1080/07055900.2016.1158145>
- Damien, P., Bianchi, D., Kessouri, F., & McWilliams, J. C. (2023). Modulation of phytoplankton uptake by mesoscale and submesoscale eddies in the California current system. *Geophysical Research Letters*, *50*(16), e2023GL104853. <https://doi.org/10.1029/2023gl104853>
- Damien, P., Bianchi, D., McWilliams, J. C., Kessouri, F., Deutsch, C., Chen, R., & Renault, L. (2023). Enhanced biogeochemical cycling along the US west coast shelf. *Global Biogeochemical Cycles*, *37*(1), e2022GB007572. <https://doi.org/10.1029/2022gb007572>
- Dauhajre, D. P., McWilliams, J. C., & Uchiyama, Y. (2017). Submesoscale coherent structures on the continental shelf. *Journal of Physical Oceanography*, *47*(12), 2949–2976. <https://doi.org/10.1175/jpo-d-16-0270.1>
- Davis, K. A., Banas, N. S., Giddings, S. N., Siedlecki, S. A., MacCready, P., Lessard, E. J., et al. (2014). Estuary-enhanced upwelling of marine nutrients fuels coastal productivity in the US Pacific Northwest. *Journal of Geophysical Research: Oceans*, *119*(12), 8778–8799. <https://doi.org/10.1002/2014jc010248>
- Desmet, F., Gruber, N., Köhn, E. E., Münnich, M., & Vogt, M. (2022). Tracking the space-time evolution of ocean acidification extremes in the California current system and northeast Pacific. *Journal of Geophysical Research: Oceans*, *127*(5), e2021JC018159. <https://doi.org/10.1029/2021jc018159>
- Desmet, F., Münnich, M., & Gruber, N. (2023). Spatiotemporal heterogeneity in the increase of ocean acidity extremes in the northeast Pacific. *Biogeosciences Discussions*, *2023*, 1–36.
- Deutsch, C., Berelson, W., Thunell, R., Weber, T., Tems, C., McManus, J., et al. (2014). Centennial changes in north Pacific anoxia linked to tropical trade winds. *Science*, *345*(6197), 665–668. <https://doi.org/10.1126/science.1252332>
- Deutsch, C., Brix, H., Ito, T., Frenzel, H., & Thompson, L. (2011). Climate-forced variability of ocean hypoxia. *Science*, *333*(6040), 336–339. <https://doi.org/10.1126/science.1202422>
- Deutsch, C., Ferrel, A., Seibel, B., Pörtner, H.-O., & Huey, R. B. (2015). Climate change tightens a metabolic constraint on marine habitats. *Science*, *348*(6239), 1132–1135. <https://doi.org/10.1126/science.aaa1605>
- Deutsch, C., Frenzel, H., McWilliams, J. C., Renault, L., Kessouri, F., Howard, E., et al. (2021). Biogeochemical variability in the California current system. *Progress in Oceanography*, *196*, 102565. <https://doi.org/10.1016/j.pocan.2021.102565>
- Doney, S. C., Fabry, V. J., Feely, R. A., & Kleypas, J. A. (2009). Ocean acidification: The other CO₂ problem. *Annual Review of Marine Science*, *1*, 169–192. <https://doi.org/10.1146/annurev.marine.010908.163834>
- Evans, N., Schroeder, I. D., Pozo Buil, M., Jacox, M. G., & Bograd, S. J. (2020). Drivers of subsurface deoxygenation in the southern California current system. *Geophysical Research Letters*, *47*(21), e2020GL089274. <https://doi.org/10.1029/2020gl089274>
- Fabry, V. J., Seibel, B. A., Feely, R. A., & Orr, J. C. (2008). Impacts of ocean acidification on marine fauna and ecosystem processes. *ICES Journal of Marine Science*, *65*(3), 414–432. <https://doi.org/10.1093/icesjms/fsn048>
- Feely, R. A., Alin, S., Carter, B., Bednaršek, N., Hales, B., Chan, F., et al. (2016). Chemical and biological impacts of ocean acidification along the west coast of north America. *Estuarine, Coastal and Shelf Science*, *183*, 260–270. <https://doi.org/10.1016/j.ecss.2016.08.043>
- Feely, R. A., Carter, B. R., Alin, S. R., Greeley, D., & Bednaršek, N. (2024). The combined effects of ocean acidification and respiration on habitat suitability for marine calcifiers along the west coast of north America. *Journal of Geophysical Research: Oceans*, *129*(4), e2023JC019892. <https://doi.org/10.1029/2023jc019892>
- Feely, R. A., Doney, S. C., & Cooley, S. R. (2009). Ocean acidification: Present conditions and future changes in a high-co world. *Oceanography*, *22*(4), 36–47. <https://doi.org/10.5670/oceanog.2009.95>
- Feely, R. A., Okazaki, R. R., Cai, W.-J., Bednaršek, N., Alin, S. R., Byrne, R. H., & Fassbender, A. (2018). The combined effects of acidification and hypoxia on pH and aragonite saturation in the coastal waters of the California current ecosystem and the northern gulf of Mexico. *Continental Shelf Research*, *152*, 50–60. <https://doi.org/10.1016/j.csr.2017.11.002>
- Feely, R. A., Sabine, C. L., Hernandez-Ayon, J. M., Janson, D., & Hales, B. (2008). Evidence for upwelling of corrosive “acidified” water onto the continental shelf. *Science*, *320*(5882), 1490–1492. <https://doi.org/10.1126/science.1155676>
- Fennel, K., Hu, J., Laurent, A., Marta-Almeida, M., & Hetland, R. (2013). Sensitivity of hypoxia predictions for the northern gulf of Mexico to sediment oxygen consumption and model nesting. *Journal of Geophysical Research: Oceans*, *118*(2), 990–1002. <https://doi.org/10.1002/jgrc.20077>
- Fennel, K., & Testa, J. M. (2019). Biogeochemical controls on coastal hypoxia. *Annual Review of Marine Science*, *11*(1), 105–130. <https://doi.org/10.1146/annurev-marine-010318-095138>
- Franco, A. C., Janson, D., Ross, T., Hannah, C., Sastri, A., & Tortell, P. D. (2023). Drivers and potential consequences of observed extreme hypoxia along the Canadian Pacific continental shelf. *Geophysical Research Letters*, *50*(6), e2022GL101857. <https://doi.org/10.1029/2022gl101857>
- Frieder, C. A., Gonzalez, J. P., Bockmon, E. E., Navarro, M. O., & Levin, L. A. (2014). Can variable pH and low oxygen moderate ocean acidification outcomes for mussel larvae? *Global Change Biology*, *20*(3), 754–764. <https://doi.org/10.1111/gcb.12485>
- Frieder, C. A., Kessouri, F., Ho, M., Sutula, M., Bianchi, D., McWilliams, J. C., et al. (2023). *Effects of urban eutrophication on pelagic habitat capacity in the southern California bight*. Authorea Preprints.
- Frieder, C. A., Nam, S., Martz, T., & Levin, L. (2012). High temporal and spatial variability of dissolved oxygen and pH in a nearshore California kelp forest. *Biogeosciences*, *9*(10), 3917–3930. <https://doi.org/10.5194/bg-9-3917-2012>
- Gruber, N., Boyd, P. W., Frölicher, T. L., & Vogt, M. (2021). Biogeochemical extremes and compound events in the ocean. *Nature*, *600*(7889), 395–407. <https://doi.org/10.1038/s41586-021-03981-7>
- Gruber, N., Hauri, C., Lachkar, Z., Loher, D., Frölicher, T. L., & Plattner, G.-K. (2012). Rapid progression of ocean acidification in the California current system. *Science*, *337*(6091), 220–223. <https://doi.org/10.1126/science.1216773>
- Haigh, R., Janson, D., Holt, C. A., Neate, H. E., & Edwards, A. M. (2015). Effects of ocean acidification on temperate coastal marine ecosystems and fisheries in the northeast Pacific. *PLoS One*, *10*(2), e0117533. <https://doi.org/10.1371/journal.pone.0117533>
- Hales, B., Karp-Boss, L., Perlin, A., & Wheeler, P. A. (2006). Oxygen production and carbon sequestration in an upwelling coastal margin. *Global Biogeochemical Cycles*, *20*(3). <https://doi.org/10.1029/2005gb002517>
- Harris, K. E., DeGrandpre, M. D., & Hales, B. (2013). Aragonite saturation state dynamics in a coastal upwelling zone. *Geophysical Research Letters*, *40*(11), 2720–2725. <https://doi.org/10.1002/grl.50460>

- Hauri, C., Gruber, N., McDonnell, A., & Vogt, M. (2013). The intensity, duration, and severity of low aragonite saturation state events on the California continental shelf. *Geophysical Research Letters*, *40*(13), 3424–3428. <https://doi.org/10.1002/grl.50618>
- Hauri, C., Gruber, N., Plattner, G.-K., Alin, S., Feely, R. A., Hales, B., & Wheeler, P. A. (2009). Ocean acidification in the California current system. *Oceanography*, *22*(4), 60–71. <https://doi.org/10.5670/oceanog.2009.97>
- Hauri, C., Gruber, N., Vogt, M., Doney, S. C., Feely, R. A., Lachkar, Z., et al. (2013). Spatiotemporal variability and long-term trends of ocean acidification in the California current system. *Biogeosciences*, *10*(1), 193–216. <https://doi.org/10.5194/bg-10-193-2013>
- Hickey, B. M., & Banas, N. S. (2008). Why is the northern end of the California Current System so productive? *Oceanography*, *21*(4), 90–107. <https://doi.org/10.5670/oceanog.2008.07>
- Howard, E. M., Penn, J. L., Frenzel, H., Seibel, B. A., Bianchi, D., Renault, L., et al. (2020). Climate-driven aerobic habitat loss in the California current system. *Science Advances*, *6*(20), eaay3188. <https://doi.org/10.1126/sciadv.aay3188>
- Hypolite, D., Romero, L., McWilliams, J. C., & Dauhahre, D. P. (2021). Surface gravity wave effects on submesoscale currents in the open ocean. *Journal of Physical Oceanography*, *51*(11), 3365–3383. <https://doi.org/10.1175/jpo-d-20-0306.1>
- IPCC. (2023). In H. Lee & H. Romero (Eds.), *Climate Change 2023: Synthesis Report. Contribution of Working Groups I, II and III to the Sixth Assessment Report of the Intergovernmental Panel on Climate Change [core writing team]* (pp. 35–115). <https://doi.org/10.59327/IPCC/AR6-9789291691647>
- Jacox, M., Moore, A., Edwards, C., & Fiechter, J. (2014). Spatially resolved upwelling in the California current system and its connections to climate variability. *Geophysical Research Letters*, *41*(9), 3189–3196. <https://doi.org/10.1002/2014gl059589>
- Jiang, L.-Q., Feely, R. A., Wanninkhof, R., Greeley, D., Barbero, L., Alin, S., et al. (2021). Coastal ocean data analysis product in north America (codap-na)—an internally consistent data product for discrete inorganic carbon, oxygen, and nutrients on the us north American ocean margins. *Earth System Science Data Discussions*, *2021*, 1–29.
- Juranek, L., Feely, R., Peterson, W., Alin, S., Hales, B., Lee, K., et al. (2009). A novel method for determination of aragonite saturation state on the continental shelf of central Oregon using multi-parameter relationships with hydrographic data. *Geophysical Research Letters*, *36*(24). <https://doi.org/10.1029/2009gl040778>
- Kessouri, F., Bianchi, D., Renault, L., McWilliams, J. C., Frenzel, H., & Deutsch, C. (2020). Submesoscale currents modulate the seasonal cycle of nutrients and productivity in the California Current System. *Global Biogeochemical Cycles*, *34*(10), e2020GB006578. <https://doi.org/10.1029/2020gb006578>
- Kessouri, F., McLaughlin, K., Sutula, M., Bianchi, D., Ho, M., McWilliams, J. C., et al. (2021). Configuration and validation of an oceanic physical and biogeochemical model to investigate coastal eutrophication in the southern California bight. *Journal of Advances in Modeling Earth Systems*, *13*(12), e2020MS002296. <https://doi.org/10.1029/2020ms002296>
- Kessouri, F., McWilliams, C. J., Deutsch, C., Renault, L., Frenzel, H., Bianchi, D., & Molemaker, J. (2020). Roms-vec oceanic physical and biogeochemical model code for the southern California current system v2020 [Software]. *Zenodo*. <https://doi.org/10.5281/zenodo.3988618>
- Kessouri, F., McWilliams, J. C., Bianchi, D., Sutula, M., Renault, L., Deutsch, C., et al. (2021). Coastal eutrophication drives acidification, oxygen loss, and ecosystem change in a major oceanic upwelling system. *Proceedings of the National Academy of Sciences of the United States of America*, *118*(21), e2018856118. <https://doi.org/10.1073/pnas.2018856118>
- Key, R. M., Kozyr, A., Sabine, C. L., Lee, K., Wanninkhof, R., Bullister, J. L., et al. (2004). A global ocean carbon climatology: Results from global data analysis project (glodap). *Global Biogeochemical Cycles*, *18*(4). <https://doi.org/10.1029/2004gb002247>
- Kroeker, K. J., Donham, E. M., Vylet, K., Warren, J. K., Cheresih, J., Fiechter, J., et al. (2023). Exposure to extremes in multiple global change drivers: Characterizing ph, dissolved oxygen, and temperature variability in a dynamic, upwelling dominated ecosystem. *Limnology & Oceanography*, *68*(7), 1611–1623. <https://doi.org/10.1002/lno.12371>
- Laruelle, G. G., Cai, W.-J., Hu, X., Gruber, N., Mackenzie, F. T., & Regnier, P. (2018). Continental shelves as a variable but increasing global sink for atmospheric carbon dioxide. *Nature Communications*, *9*(1), 454. <https://doi.org/10.1038/s41467-017-02738-z>
- Laruelle, G. G., Dürr, H., Lauerwald, R., Hartmann, J., Slomp, C., Goossens, N., & Regnier, P. (2013). Global multi-scale segmentation of continental and coastal waters from the watersheds to the continental margins. *Hydrology and Earth System Sciences*, *17*(5), 2029–2051. <https://doi.org/10.5194/hess-17-2029-2013>
- Laurent, A., Fennel, K., Cai, W.-J., Huang, W.-J., Barbero, L., & Wanninkhof, R. (2017). Eutrophication-induced acidification of coastal waters in the northern gulf of Mexico: Insights into origin and processes from a coupled physical-biogeochemical model. *Geophysical Research Letters*, *44*(2), 946–956. <https://doi.org/10.1002/2016gl071881>
- Levin, L. A. (2018). Manifestation, drivers, and emergence of open ocean deoxygenation. *Annual Review of Marine Science*, *10*(1), 229–260. <https://doi.org/10.1146/annurev-marine-121916-063359>
- Li, G., Cheng, L., Zhu, J., Trenberth, K. E., Mann, M. E., & Abraham, J. P. (2020). Increasing ocean stratification over the past half-century. *Nature Climate Change*, *10*(12), 1116–1123. <https://doi.org/10.1038/s41558-020-00918-2>
- Liu, X., Dunne, J. P., Stock, C. A., Harrison, M. J., Adcroft, A., & Resplandy, L. (2019). Simulating water residence time in the Coastal Ocean: A global perspective. *Geophysical Research Letters*, *46*(23), 13910–13919. <https://doi.org/10.1029/2019gl085097>
- Liu, X., Stock, C. A., Dunne, J. P., Lee, M., Shevliakova, E., Malyshev, S., & Milly, P. C. (2021). Simulated global coastal ecosystem responses to a half-century increase in river nitrogen loads. *Geophysical Research Letters*, *48*(17), e2021GL094367. <https://doi.org/10.1029/2021gl094367>
- Locarnini, M., Mishonov, A., Baranova, O., Boyer, T., Zweng, M., Garcia, H., et al. (2018). World ocean atlas 2018, volume 1: Temperature. McClatchie, S., Goericke, R., Cosgrove, R., Auad, G., & Vetter, R. (2010). Oxygen in the southern California bight: Multidecadal trends and implications for demersal fisheries. *Geophysical Research Letters*, *37*(19). <https://doi.org/10.1029/2010gl014497>
- Moore, J. K., Doney, S. C., & Lindsay, K. (2004). Upper ocean ecosystem dynamics and iron cycling in a global three-dimensional model. *Global Biogeochemical Cycles*, *18*(4). <https://doi.org/10.1029/2004gb002220>
- Muller-Karger, F. E., Varela, R., Thunell, R., Luerssen, R., Hu, C., & Walsh, J. J. (2005). The importance of continental margins in the global carbon cycle. *Geophysical Research Letters*, *32*(1). <https://doi.org/10.1029/2004gl021346>
- Olsen, A., Key, R. M., Van Heuven, S., Lauvset, S. K., Velo, A., Lin, X., et al. (2016). The global ocean data analysis project version 2 (glodapv2)—an internally consistent data product for the world ocean. *Earth System Science Data*, *8*(2), 297–323. <https://doi.org/10.5194/essd-8-297-2016>
- Orr, J. C., Fabry, V. J., Aumont, O., Bopp, L., Doney, S. C., Feely, R. A., et al. (2005). Anthropogenic ocean acidification over the twenty-first century and its impact on calcifying organisms. *Nature*, *437*(7059), 681–686. <https://doi.org/10.1038/nature04095>
- Oschlies, A., Brandt, P., Stramma, L., & Schmidtko, S. (2018). Drivers and mechanisms of ocean deoxygenation. *Nature Geoscience*, *11*(7), 467–473. <https://doi.org/10.1038/s41561-018-0152-2>
- Peterson, J. O., Morgan, C. A., Peterson, W. T., & Lorenzo, E. D. (2013). Seasonal and interannual variation in the extent of hypoxia in the northern California current from 1998–2012. *Limnology & Oceanography*, *58*(6), 2279–2292. <https://doi.org/10.4319/lno.2013.58.6.2279>

- Pierce, S. D., Barth, J. A., Shearman, R. K., & Erofeev, A. Y. (2012). Declining oxygen in the northeast Pacific. *Journal of Physical Oceanography*, 42(3), 495–501. <https://doi.org/10.1175/jpo-d-11-0170.1>
- Rabalais, N. N., Turner, R. E., & Wiseman Jr, W. J. (2002). Gulf of Mexico hypoxia, aka “the dead zone”. *Annual Review of Ecology and Systematics*, 33(1), 235–263. <https://doi.org/10.1146/annurev.ecolsys.33.010802.150513>
- Renault, L., McWilliams, J. C., Jousse, A., Deutsch, C., Frenzel, H., Kessouri, F., & Chen, R. (2021). The physical structure and behavior of the California current system. *Progress in Oceanography*, 195, 102564. <https://doi.org/10.1016/j.pocean.2021.102564>
- Resplandy, L., Müller, J., Najjar, R., Bianchi, D., Weber, T., Cai, W.-J., et al. (2024). A synthesis of global coastal ocean greenhouse gas fluxes. *Global Biogeochemical Cycles*, 38(1), e2023GB007803. <https://doi.org/10.1029/2023gb007803>
- Sabine, C. L., Feely, R. A., Gruber, N., Key, R. M., Lee, K., Bullister, J. L., et al. (2004). The oceanic sink for anthropogenic CO₂. *Science*, 305(5682), 367–371. <https://doi.org/10.1126/science.1097403>
- Sarmiento, J. L., & Gruber, N. (2006). *Ocean biogeochemical dynamics*. Princeton University Press.
- Schmidtko, S., Stramma, L., & Visbeck, M. (2017). Decline in global oceanic oxygen content during the past five decades. *Nature*, 542(7641), 335–339. <https://doi.org/10.1038/nature21399>
- Service, R. F. (2004). *New dead zone off Oregon coast hints at sea change in currents*. American Association for the Advancement of Science.
- Shchepetkin, A. F., & McWilliams, J. C. (2005). The regional oceanic modeling system (ROMS): A split-explicit, free-surface, topography-following-coordinate oceanic model. *Ocean Modelling*, 9(4), 347–404. <https://doi.org/10.1016/j.ocemod.2004.08.002>
- Siedlecki, S. A., Banas, N. S., Davis, K. A., Giddings, S., Hickey, B. M., MacCready, P., et al. (2015). Seasonal and interannual oxygen variability on the Washington and Oregon continental shelves. *Journal of Geophysical Research: Oceans*, 120(2), 608–633. <https://doi.org/10.1002/2014jc010254>
- Skamarock, W. C., Klemp, J. B., Dudhia, J., Gill, D. O., Barker, D. M., Duda, M. G., et al. (2008). G: A description of the advanced research WRF version 3 NCAR Tech. Note NCAR/TN-475+ STR.
- Turi, G., Lachkar, Z., Gruber, N., & Münnich, M. (2016). Climatic modulation of recent trends in ocean acidification in the California current system. *Environmental Research Letters*, 11(1), 014007. <https://doi.org/10.1088/1748-9326/11/1/014007>
- Van Heuven, S., Pierrot, D., Rae, J., Lewis, E., & Wallace, D. (2011). *Co2sys v 1.1, matlab program developed for CO₂ system calculations*. ORNL/CDIAC-105b, Carbon Dioxide Information Analysis Center, Oak Ridge National Lab. US DoE. Retrieved from <https://github.com/jamesorr/CO2SYS-MATLAB>
- Van Oostende, N., Dussin, R., Stock, C., Barton, A., Curchitser, E., Dunne, J. P., & Ward, B. (2018). Simulating the ocean's chlorophyll dynamic range from coastal upwelling to oligotrophy. *Progress in Oceanography*, 168, 232–247. <https://doi.org/10.1016/j.pocean.2018.10.009>
- Walter, R. K., Dalsin, M., Mazzini, P. L., & Pianca, C. (2024). Compound marine cold spells and hypoxic events in a nearshore upwelling system. *Estuarine, Coastal and Shelf Science*, 300, 108706. <https://doi.org/10.1016/j.ecss.2024.108706>
- Wanninkhof, R. (1992). Relationship between wind speed and gas exchange over the ocean. *Journal of Geophysical Research*, 97(C5), 7373–7382. <https://doi.org/10.1029/92jc00188>
- Zhou, F., Chai, F., Huang, D., Xue, H., Chen, J., Xiu, P., et al. (2017). Investigation of hypoxia off the Changjiang estuary using a coupled model of roms-cosine. *Progress in Oceanography*, 159, 237–254. <https://doi.org/10.1016/j.pocean.2017.10.008>